AN ABSTRACT OF THE THESIS OF

Andrew G. Miller for the degree of Master of Science in Biological and Ecological Engineering presented on June 6, 2018.

Title: Microbial Electrolysis Cells for the Production of Hydrogen Gas: Evaluation of Internal Resistance and Design for Scale-Up

Abstract approved:

_____

Hong Liu

Modification of microbial electrolysis cells (MECs) by altering the sizes of the anode and the cathode, or their interaction with the liquid stream affects the performance of the MEC, but it remains difficult to quantify how much each change will contribute to the overall performance. Through this study, a method for quantifying the effects of design decisions on internal resistance was applied for the first time to MECs. The anode surface area (15 cm^2) was the most limiting factor when phosphate buffer concentrations were greater than 50 mM. Increasing the anode surface area by layering carbon cloth was found to be an effective way to relieve this hindrance. The cathode surface area contributed less to the internal resistance, due to the use of a highly effective Molybdenum Phosphide (MoP) catalyst. Additionally, inducing fluid motion between the electrodes enhanced performance, whereas varying the spacing of the electrodes (all spacings < 1 cm) was found, surprisingly, to have little effect.

The maximum cathodic current density achieved with this design was 47 A/m^2, with a hydrogen (H_2) production rate of 3.7 L/ L-liquid volume/day. Highest

performance was obtained with an anode to cathode surface area ratio of just larger than 3.5 : 1, which was the optimal ratio predicted through the internal resistance dissection procedure. The internal resistance relation was used to adequately predict the electrical performance of two MECs from other studies. This method gives an in-depth understanding of the distribution of internal resistance, which enables design of MECs and their operational conditions for high performance.

MECs with volumes greater than one liter have been recently developed and tested, with a few demonstrating high current density and H_2-production rates. However, many of the designs shown to give the best performance are difficult to scale-up further. In the present study a highly scalable 10 L MEC was designed and evaluated. The shape of the reactor and the orientation of the electrodes encourage high fluid mixing, and the sheet metal electrode frames provide both structural support and distributed electrical connection. Solid-core insulated copper wires were found to be suitable for bringing the concentrated electrical current to and from the electrode frames. With a comparable surface area to volume ratio (30 m^2/m^3), the current density (970 A/m^3) was higher than all MEC reactors of the same size range, to the best of our knowledge. The observed current density was accurately predicted based on the internal resistance results of small scale MEC testing (0.15L), demonstrating that the electrical current scaled directly from the smaller scale. A volumetric H_2-production rate of 5.9 L/L/d was achieved. Further analysis provided some evidence that location of an electrode pair next to a reactor wall decreased current density (~ 20%), as did separating the electrodes with J-Cloth and narrower electrode spacing, rather than without a separator (~30%).

©Copyright by Andrew G. Miller
June 6, 2018
All Rights Reserved

Microbial Electrolysis Cells for the Production of Hydrogen Gas: Evaluation of Internal Resistance and Design for Scale-Up

by
Andrew G. Miller

A THESIS

submitted to

Oregon State University

in partial fulfillment of
the requirements for the
degree of

Master of Science

Presented June 6, 2018
Commencement June 2018

Master of Science thesis of Andrew G. Miller presented on June 6, 2018

APPROVED:

Major Professor, representing Biological and Ecological Engineering

Head of the Department of Biological and Ecological Engineering

Dean of the Graduate School

I understand that my thesis will become part of the permanent collection of Oregon State University libraries. My signature below authorizes release of my thesis to any reader upon request.

Andrew G. Miller, Author

ACKNOWLEDGEMENTS

I would like to express my sincere gratitude to Dr. Hong Liu for her enthusiastic pursuit of useful research. Every day I learn from her expert ability to bring forward the most important points. I really appreciate the trust that she puts in my work and her desire for me to develop as many skills as possible for the future.

I want to thank the other members of my committee, especially Dr. Frank Chaplen, for their insight and perspective on my research challenges.

I am grateful to all of my friends from the lab, and especially Luguang Wang, Ningshengjie (Grace) Gao, Dr. Lakhveer (Lucki) Singh, Gouri Mahadwar, and Stephanie Trujillo. Luguang always makes time to help me in the lab, and his attitude helps make the work more fun and productive! Lucki has been a mentor and a friend to me. We have spent many hours figuring out how to get the reactor working and getting to know each other. Grace can be counted on to help me split up long hours of work with a great comment or thought.

My roommates, Scott Heffernan, James (Jimmy) Budiac, Nicolette (Nikki) Ratz, and Isaac Sandlin, have all added so much to my experience here in Corvallis. Graduate school would have been much more difficult and less enriching without the environment that we created at the house.

Finally, I want to thank my dad, mom, and sister. My dad always has great stories and suggestions, and I feel his support strongly. My mom is so helpful and always looks out for me. My sister, Claire, is a great friend and I look forward to seeing her more once I leave university.

CONTRIBUTION OF AUTHORS

Ningshengjie Gao assisted with the electrochemical impedance spectroscopy testing and interpretation for chapter 1. Luguang Wang assisted in the construction of microbial electrolysis cells for chapters 2 and 3. Dr. Lakhveer Singh assisted with the construction and operation of the microbial electrolysis cell reactor for chapter 3. Additionally, Dr. Singh assisted with the organization and form of the writing in chapters 2 and 3.

TABLE OF CONTENTS

Page

1 General Introduction …….……1

2 Linking Internal Resistance with Design Decisions in MECs…..……..…4

2.1 Introduction……..4

2.2 Materials and Methods...……..7

2.2.1 Reactor Construction…….…7

2.2.2 Inoculum & Catalyst Preparation…….……..8

2.2.3 Experimental Operation…….8

2.2.4 Chemical & Electrical Measurement ……..……..9

2.2.5 Performance Calculations ……...……10

2.2.6 Internal Resistance Analysis Method …...……...……11

2.3 Results and Discussion...……...14

2.3.1 Relative Impact of Design Factors on Performance…….…...14

2.3.2 Investigating Performance-Limiting Electrode……17

2.3.3 Relationship Between H_2-Production and Current Density….18

2.3.4 Dissecting Internal Resistance…….21

2.3.5 Predicting Performance of Other Studies…….....27

2.4 Implications……29

2.5 References…….....30

TABLE OF CONTENTS (Continued)

Page

3 Scaled-up MEC Reactor Design and Evaluation …..…….…….33

3.1 Introduction……33

3.2 Materials and Methods...……37

3.2.1 Reactor Design…….……37

3.2.2 Anode Innoculation and Cathode Catalyst……..38

3.2.3 Immobilized Fermentative Bacterial Beads…….38

3.2.4 Reactor Configurations……39

3.2.5 Reactor Operation and Measurement……...40

3.2.6 Performance Calculations……41

3.3 Results and Discussion...……...42

3.3.1 Impact of Wiring Choice on Current Output……...…42

3.3.2 Influence of Cloth Separator and Electrode Spacing……...44

3.3.3 Effect of MEC Location in Reactor…….45

3.3.4 H_2-Production Performance…….47

3.3.5 Effect of Scale-Up on Current Density……48

3.4 Implications……50

3.5 References……..52

4 Conclusions……...……54

TABLE OF CONTENTS (Continued)

Page

Bibliography……..……..57

Appendices ……...…….……..62

Appendix A...……..…….63

Small-Scale MEC Images……63

Characterization of Fluid Mixing Condition……64

Electrochemical Impedance Spectroscopy (EIS) Analysis……..66

Assumptions about MECs for Performance Prediction……...69

Appendix B……..……70

10 L Reactor Images……70

Comparison of MEC Reactor Performance with Other Studies……..71

LIST OF FIGURES

Figure Page

2.1: MECs operated with differing electrode spacing, buffer concentration, and mixing condition…..…….....15

2.2: Current density based on smaller electrode for MECs with various anode to cathode surface area ratios …….…….…….18

2.3: Example batch behavior for MEC without and with treatment to prevent H_2-consumption …….20

2.4: Voltage required for the a range of electrical currents for five MECs with various anode to cathode surface area ratios, and buffer concentrations …...….22

2.5: Current of various MECs not used to train the internal resistance model compared to predicted current ……...…….26

2.6: Subsection of the observed data from two different studies compared to the performance predicted...……28

3.1: Reactor setup showing recirculation tank for heating liquid, pumps, power supply, and liquid-gas separation flask ……....37

3.2: Diagram of reactor electrode configurations with recirculation inlets and outlets shown …….41

3.3: Startup of MEC reactor showing change of electrode wiring……..43

3.3: Reactor operated in 3C configuration at a range of input voltages ...……..45

3.4: Reactor operated in 5C configuration 24 h retention time and 12 h retention time ……...……46

3.5: Current density predicted for high and low mixing condition, compared to the measured values for the 3C configuration ……...49

LIST OF TABLES

Table Page

2.1: Internal resistance model results for both mixing conditions ……..23

LIST OF APPENDIX FIGURES

Figure Page

2.7: Side view of example MEC, showing anode biofilm,
titanium wires, and liquid level ……...63

2.8: Front view of example MEC, showing electrode spacing ….……..64

2.9. Typical EIS nyquist plot …….…….……67

3.7: Photo of 10 L reactor and diagram of electrodes before clamping ……..70

3.8: Front view of 5C configuration, showing electrode spacing……71

LIST OF APPENDIX TABLES

Table Page

2.2: Ionic/ohmic resistance for small-scale MEC with
medium and wide spacing, compared with other studies …….…..68

2.3: Approximation of design of MECs in other studies
for use in internal resistance prediction model ……...……....69

3.1: Comparison of 10 L reactor performance with other studies …….…….72

Chapter 1: General Introduction

Continuing to consume fossil fuel-based energy at current levels is not a path toward a prosperous future for the world's inhabitants. This is due largely, but not only, to the reality of climate change. While the most critical steps in the immediate future are to reduce energy-consumption where possible, it is also greatly beneficial to invest in creating a viable long-term energy portfolio. Hydrogen gas (H_2) is one of the most promising options as a transportation fuel for many reasons, including that it is clean burning and can be pumped rapidly into a vehicle. There is ongoing debate about which types of transportation and in which scenarios H_2 or electricity is more suitable (Jorgensen, 2008). However, for H_2 to be a true alternative to fossil fuels it must be produced renewably. In 2012 about 96% of H_2 was produced from fossil fuels and 4% was produced from water power (Ursua et al., 2012). Microbial electrolysis cells (MECs) are a recently developed technology that can generate H_2 efficiently, which may play a role in the future energy system.

At the core of each MEC is a biofilm of microorganisms that can digest dissolved organic material in liquid streams, but only when there is a solid material nearby that can receive the electrons produced during this metabolism. This category of bacteria has been named 'exoelectrogens', due to their ability to transfer electrons from within their cell wall to a material outside of their cell wall. During operation of a MEC, a voltage is applied between a second electrode, the cathode, and the electrode where the exoelectrogens are living, the anode. This voltage pulls the electrons away from the anode, allowing the microbes to keep metabolizing the

organic material. At the same time, the applied voltage helps to combine the electrons with H^+ ions, protons, to form H_2 at the cathode.

In this way, the bacteria serve a similar role as a chemical catalyst. They 'unlock' an electron from a compound with significant chemical energy (dissolved organic material) and this electron requires only a small additional amount of energy to combine with the protons. Whereas water hydrolysis, a process where a voltage is applied between two electrodes in water to generate H_2, typically uses an input voltage of greater than 1.6 V, a MEC typically uses only about 0.7 – 1 V (Kadier et al., 2016). Most MECs operated at a lower applied voltage than 1.1 V, for a variety of waste streams, recover a higher amount of energy (in H_2 fuel) than was input (as electricity) (Lu and Ren, 2016). So, the efficiency of H_2 production, based on electricity, in MECs is greater than 100%, often about 150%, whereas most water hydrolysis produces H_2 fuel at about 60-80% efficiency (Ursua et al., 2012).

A second benefit that comes with harvesting the energy within oxidizable organic chemicals is that the concentrations of these chemicals can be greatly reduced (Rozendal et al., 2008). Oxidizable organic chemicals at high concentrations are considered pollutants, since they draw down the dissolved O_2 concentrations in the water bodies in which they are disposed, harming wildlife. In fact, the strongest pull for the initial implementation of MECs is likely to be their contribution to a low operating cost for wastewater treatment. Fuel produced by the MEC can be used on-site to power the wastewater treatment. MECs, as well as the closely related microbial fuel cell (MFC), produce very little waste sludge, which is an advantage over conventional wastewater treatment systems, in which the treatment and disposal of sludge is a major operating cost (Brown et al., 2015; Wilson and Kim, 2016). When compared in a scenario

of treating winery wastewater, H_2-producing MECs were found to be more likely suitable, economically, than the electricity-producing MFCs (Cusick et al., 2010).

The next step for finding a feasible role for MECs is scale-up. A few proof-of-concept tests of MECs with volumes larger than 100 L have been conducted that have resulted in successful water treatment and some fuel recovery (Cotterill S. E. et al., 2017; Cusick et al., 2011). However, even for reactors of only a few liters, the volumetric hydrogen production rates have been one to two orders of magnitude lower than that of small reactors (volume 0.1 L or less) (Lu and Ren, 2016). There is substantial need for a study on the resistances that restrict high performance in MECs and how a scalable reactor can be designed to alleviate these.

Chapter 2: Linking Internal Resistance with Design Decisions in MECs

2.1 INTRODUCTION

MECs have the potential to serve two very different roles: as a mechanism for recovering unused energy from waste streams while lowering their organic content, and as a device for producing a surplus of high-value H_2 fuel. It remains to be seen whether it is most suitable as an energy recovery wastewater treatment module or as a circular-economy production device. In either case, central to MEC success is for their material cost to be decreased. Capital cost is most directly addressed by increasing the production rate of H_2. Increasing it relative to the electrode surface area decreases the amount of electrode materials needed, while increasing it relative to the volume decreases the footprint and size of the final product. The introduction of a single chamber design improved MEC performance relative to both surface area and volume (Hu et al., 2008).

Many modifications to MEC design have been tested in pursuit of improving performance. H_2-production rates of a MEC at a given operating condition have typically been found to be closely related to its current density (Dudley et al., 2018). Changing the reactor design through different placement of the cathode and anode increased the current density of the MECs (Gil-Carrera et al., 2011; Liang et al., 2011). Another method that is often mentioned for improving performance in MECs is decreasing electrode spacing (Kadier et al., 2016; Ki et al., 2016). Cheng and Logan (2011) found that decreasing the electrode spacing to 2 cm improved the reactor performance, and they argued that decreasing the spacing to 1 cm would have further

improved performance, except for a low-surface-area anode capping the performance at similar levels. A number of other studies focused on increasing the anode surface area, which was most often accomplished by switching to a thicker type of anode material, such as carbon brush or carbon felt, that has a larger surface area within the fibers (Barbosa et al., 2018; Call and Logan, 2008). The physical interaction of the solution with the electrodes was shown to be important in studies on flow-through anodes and fluidized particles of granular activated carbon (Liu et al., 2014; Sleutels et al., 2009b). While there is a solid foundation of studies showing methods to improve MEC performance, there is still a need for studies that quantify and compare the effect of different design decisions.

Internal resistance can be quantified for comparing MEC designs and performance. Internal resistance, although defined in multiple ways, relates the amount of electrical current within a MEC to the input voltage. Some studies simply divide the electrical current by the input voltage to find an ‘apparent resistance’, but this value does not represent an intrinsic property of the MEC, since the apparent resistance differs based on the input voltage used (P. Borole and J. Lewis, 2017; Tartakovsky et al., 2011). Simple methods to measure overall internal resistance include increasing the input voltage by steps over a period of about an hour and measuring the slope of the current versus the input voltage (Tartakovsky et al., 2009).

Quantifying the internal resistance associated with different aspects of a MEC can provide more explanation for the resistance difference among designs. Many studies characterize the relationship between input voltage and current in MECs as involving ‘overpotentials’ for the anode and cathode and ‘solution resistance’. The overpotentials of the electrodes are due to the processes of (bio)chemical kinetics (also called charge transfer effects) and mass transfer (also called concentration effects). The ‘solution/ohmic resistance’ is due to transferring ions between

the electrodes (Ki et al., 2016; P. Borole and J. Lewis, 2017; Sedaqatvand et al., 2013; Sleutels et al., 2009a). With this understanding, the three components of the internal resistance (resistance causing anode overpotential, resistance causing cathode overpotential, and solution resistance) are related to transfer *processes*.

The most common way to measure the contribution of different processes to internal resistance is through alternating current electrochemical analytical methods, specifically Electrochemical Impedance Spectroscopy (EIS). Use of EIS with MECs has been studied, but the veracity of the results relies on the use of the most appropriate equivalent electrical circuit. An equivalent electrical circuit is needed since EIS is an indirect way of measuring the physical processes, and there is some ongoing investigation about choosing the appropriate one (Dominguez-Benetton et al., 2012; P. Borole and J. Lewis, 2017). The overpotentials can also be measured more directly by using a reference electrode and by either doing chemical analysis or by using current-interrupt methods (Guo et al., 2017; Sleutels et al., 2013). Alternatives to an experimental determination of the impacts of design on internal resistance would be either an investigation with a mechanistic model or a co-investigation using experimental tests to fit model parameters. However, the design decisions focused on in this study mostly affect the solution-electrode interfaces, and no model has yet been developed for MECs that tackle the processes at both electrodes (Gadkari et al., 2018).

The current study compares the effect of anode surface area, cathode surface area, buffer concentration, electrode spacing, and mixing condition on the electrochemical performance of MECs. Electrode spacing of less than 1 cm was studied, as the effect of spacing distance at this range has not previously been studied, to the best of our knowledge. To further understand the role of anode and cathode surface area and solution buffer concentration, these three design

decisions were matched to a component of the MEC internal resistance for both a high and a low mixing condition. Whereas other studies highlight the limiting mechanisms (kinetics, ion transport, or diffusion), this study identifies the limiting design decision.

2.2 MATERIALS AND METHODS

2.2.1 Reactor Construction

Nine single-chamber MECs without separators were constructed in order to investigate the effect of design decision on electrochemical performance. The reactor vessels for the MECs werer narrow mouth media bottles sealed with butyl septum topped caps (VWR International, LLC). Total reactor volumes were 320 mL with a liquid volume of 150 mL and a gas volume of 170 mL. The electrodes were made of carbon cloth (Type-B, fuelcellearth.com) and connected to titanium wire by using nylon screws, nuts, and washers to ensure firm contact. The input voltage (0.4 – 1.0 V) was applied between the electrodes of the MECs by a power supply (Circuit Specialists, CSI1802X), to make the electric potentials of the anodes more positive than the cathodes. The anode and the cathode were fixed onto plastic frames and placed facing toward each other. The MECs were placed horizontally so that the electrodes were entirely under the level of the solution (Appendix A, Fig. 2.7). Each strip of carbon cloth used in the electrodes measured 1.5 cm x 10 cm (projected surface area 15 cm^2).

2.2.2 Inoculum & Catalyst Preparation

The anode biofilms were inoculated by scraping biofilm from the anode of long-term operated MECs and applying it to the surface of plain carbon cloth. The community was originally enriched from local domestic wastewater (Liu and Logan, 2004). The cathode catalyst was a MoP catalyst developed at Pacific Northwest National Lab (unpublished). The cathode was prepared as follows: (i) the MoP catalyst was mixed with Nafion (5%, Sigma–Aldrich) for 10 h in a ratio of 7 mL Nafion per mg of MoP catalyst to form a solution; (ii) the solution was applied on both sides of the cathode using a micropipette (iii) the cathode was dried at room temperature for 24 h.

2.2.3 Experimental Operation

The MECs were fed with solution containing acetate concentration of 50 mM with the following (per liter): NH_4Cl, 0.31 g; KCl, 0.13 g; and mineral (12.5 mL) and vitamin (12.5 mL) solutions as reported (Bond and Lovley, 2003). Phosphate buffer concentrations between 30 mM (1.75 g/L NaH_2PO_4, 2.46 g/L Na_2HPO_2) and 300 mM (17.5 g/L NaH_2PO_4, 24.6 g/L Na_2HPO_2) were tested.

Batch tests were used to study the limiting factors and internal resistances of the MECs. The MECs were operated for between one and four days as circuit current increased and reached a peak, and were disconnected once current remained stable or began to decrease. Temperature was maintained at 32°C. The solution was replaced at the end of each batch and before starting the new batch the headspace was purged with N_2 gas for 10 minutes to create anaerobic

conditions. The nine MECs were operated in groups of two or three and the average results over at least two batches were considered to be final.

For the tests with various electrode surface area ratios, anode : cathode surface area was changed by overlaying more pieces of one electrode without changing the other electrode. MECs with electrode surface area ratios of 1:1 (anode: cathode) had one strip of carbon cloth for each electrode, whereas for MECs with ratios of 2:1 and 1:2 (anode : cathode) the anode and cathode had two strips, respectively. The anode and cathode pieces that were added were taken directly from deconstructed functioning MECs. The electrode distance spacing was adjusted by adding one or two nylon nuts between the plastic electrode frames that support the carbon cloth and titanium electrodes, with the narrow (4 mm), medium (7 mm), and wide (9 mm) spacing having 0, 1, and 2 nuts between the plastic frames, respectively. The MECs were subjected to either 'no mixing condition', where they were stationary, or they were placed on a shaker plate (shaking diameter 10 mm) that orbited at a rate of 90 rpm. The Reynolds number associated with this fluid flow condition, as well as a discussion of the mechanisms that fluid flow affects MEC performance can be found in Appendix A. In experiments to compare electrical current to H_2-production, the consumption of H_2 was controlled through chemical treatment: chloroform ($CHCl_3$) was dissolved into the solution at a concentration of 0.02% (v/v).

2.2.4 Chemical & Electrical Measurement

During the batches, the excess gas was released at day intervals for volume measurement and composition analysis with a gas chromatograph (Agilent, 6890N; J&W Scientific, USA) equipped with a thermal conductivity detector and a column (113-3133 CARBONPLT, 30 m x

0.32mm x 3 mm, J&W Scientific, USA) with argon as the carrier gas. The volume of biogas was measured using the water replacement method. The biogas production was calculated according to the previously described method (Hu et al., 2008). Solution samples taken from representative batches in order to assess the amount of acetate leftover in the MECs. The acetate concentration was determined using a high performance liquid chromatograph (Agilent Technologies 1200 Series) equipped with Aminex HPX-87H column and a refractive index detector. The mobile phase was 0.005M sulfuric acid with a flow rate of 0.4 mL/min. The temperatures of the column and the detector were 30°C and 35°C, respectively. Injection volume for each sample was set at 10 uL. The system was calibrated with a mixture of standard volatile acids from Agilent.

The current within each MEC was measured at 7 minute intervals by a data acquisition system (2700, Keithly, USA), which recorded the voltage drop over a small resistor of known resistance (1 Ω) that was in series with the MEC. To calculate the peak current density that a MEC generated for a given batch, the maximum average of about two hours of data (18 consecutive data points over 119 min.) was used.

Electrochemical Impedance Spectroscopy (EIS) was performed on MECs with two different spacings of the electrodes, using the potentiostat (References 100, Gamry Instruments Inc., Warminster, PA). For the EIS analysis the anode was the working electrode and the cathode was both the counter and the reference electrode, and perturbations of 10 mV were used at frequencies between 100,000 Hz and 0.1 Hz, with 10 points per decade. During this ‘whole cell’ testing the MECs were at open circuit voltage (OCV).

2.2.5 Performance Calculations

Current density was calculated by dividing the current by the projected surface area of the smaller electrode (15 cm^2). In most cases, the smaller electrode was the cathode, except for the MECs with the anode to cathode surface area ratio of 1:2. The H_2 production rate was normalized by the working liquid volume of the reactor (150 mL). The cathodic H_2 recovery and the energy yield relative to electrical input were calculated as described previously (Logan et al., 2008). A gas temperature of 23°C was used, as gas volumes were measured at room temperature. The higher heat of combustion, 285.83 kJ/mol-H_2, was used for the energy yield calculation.

2.2.6 Internal Resistance Analysis Method

The simplest relationship between input voltage and electrical current within a MEC is that the required input voltage increases linearly with the amount of current. The rate that the required input voltage scales with electrical current is the equivalent electrical resistance of the system. In the present study this linear resistance was taken as the internal resistance of the MEC. The input voltage that a MEC requires to produce a current, I is therefore conceptualized as:

$$V_{input} = R_{internal} * I + V_{Zero-Current} \tag{2.1}$$

Where $V_{Zero-Current}$ is the linear approximation of the minimum voltage that is required for the coupled oxidation and reduction reactions to become favorable. MECs with the same substrate concentrations and electrode materials and coatings, but with otherwise different setup are

assumed to have the same $V_{Zero-Current}$, but different $R_{internal}$. $V_{Zero-Current}$ differs in numerical value from the actual minimum input voltage required for the MEC to begin producing electrical current or H_2 gas, due to the MEC deviating from linear behavior for low voltage inputs. Equation 2.1 is only valid for input voltages that are sufficient to produce electrical current within the MEC, and it is most suited for describing and being fit to the performance of the MEC away from the extremes of input voltage, which produce nonlinear responses in electrical current. The internal resistance term in Equation 2.1 was expanded as shown below:

$$R_{internal} = R_{Anode} + R_{Cathode} + R_{Solution} \tag{2.2}$$

Each of these resistance terms is then normalized by the relevant surface area measurement:

$$R_{Anode} = \frac{r_{An}}{S_{An}} \tag{2.3}$$

$$R_{Cathode} = \frac{r_{Cat}}{S_{Cat}} \tag{2.4}$$

$$R_{Solution} = \frac{r_{Sol}}{S_{Sol}} \tag{2.5}$$

Where r_{An}, r_{Cat}, and r_{Sol} are the area-specific resistances of the anode, cathode, and solution, respectively with the units of $[\Omega\ cm^2]$. S_{An} and S_{Cat} are the one-sided surface area of the anode and cathode electrodes, respectively, and S_{Sol} is the projected area between the two electrodes, which is occupied by solution, all with units of $[\ cm^2]$. In the case of the experiments conducted the solution surface area was always 15 cm^2. Resistance is expected to scale with the inverse of surface area, since a larger surface area or projected area allows for chemical (mass) transport and/or electron transport to occur in parallel with more locations.

The solution resistance term can be further expanded to detail the influence that the phosphate buffer concentration has on its value. Solution resistance was expected to vary with the inverse of phosphate buffer concentration, since the buffer species can act as proton-carriers that move between the electrodes. In this way the solution resistance was initially expanded as shown in Equation 2.6.

$$R_{Solution} = \frac{r_{Sol}}{S_{Sol}} = \frac{\alpha_{Sol}}{S_{Sol} * C_{buffer}} \tag{2.6}$$

where C_{buffer} is the phosphate buffer concentration in the solution and α_{Sol} is a constant that scales the term and accounts for units. C_{buffer} is in units of molar, and α_{Sol} is in units of $[\Omega\ cm^2/M]$.

The final independent variable that was studied, besides anode and cathode surface area, phosphate buffer concentration and electrode distance spacing, was mixing condition. In order to avoid making assumptions about which portion of the internal resistance shaking would affect, and whether it would affect the voltage for zero current, the values in Equation 2.7 (r_{An}, r_{Cat}, a_{Sol}, and $V_{Zero-Current}$) were fit to the non-shaking tests and separately to the shaking tests.

$$V_{Input} = \left(\frac{r_{An}}{S_{An}} + \frac{r_{Cat}}{S_{Cat}} + \frac{\alpha_{Sol}}{S_{sol} * C_{Buffer}}\right) * I + V_{Zero-Current} \tag{2.7}$$

This internal resistance model (Equation 2.7) was fit to the data using the Levenberg-Marquardt nonlinear least-squares algorithm (curve_fit fuction within the scipy.optimize package in Python). A differential evolution genetic algorithm within the same Python package was used to set the initial values for the least squares fit (differential_evolution).

2.3 RESULTS AND DISCUSSION

2.3.1 Relative Impact of Design Factors on Electrical Performance

During this section, design decisions (electrode spacing, anode and cathode surface area) and operational conditions (buffer concentration, fluid mixing condition) were varied to examine their relative importance for MECs. Adjusting the electrode spacing from 4 mm to 9 mm had very little effect on current density (Fig. 2.1). This suggests that the internal resistance was not substantially decreased. In fact, the MECs with the largest electrode spacing appeared to have the highest performance, although the overlap of the 95% confidence interval bars (+/- 2 standard error) support that this difference may be due to randomness rather than due to the electrode spacing distance. An ANOVA t-test (not shown) of the performance at 75 mM buffer found that the performance of the middle-size electrode spacing would be expected to be lower than that of the wide spacing MECs (between 0.08 – 0.8 A/m^2 lower) and either lower or higher than the narrow spacing MECs (between 0.5 A/m^2 lower and 0.2 A/m^2 higher). There was not enough evidence to show that the performance of the wide and narrow electrode spacing MECs differed, with the performance of the wide MECs being estimated as between 0.6 A/m^2 lower and 0.07 A/m^2 higher than that of the narrow MECs.

In contrast to this finding, multiple previous studies have reported that a narrower spacing between the anode and the cathode decreases internal resistance and improves MEC performance (Cheng and Logan, 2011; Liu et al., 2005). The lack of clear effect of electrode spacing on current density may relate to three aspects of our study. The first aspect is the range of spacing distances that were used: 4 mm – 9 mm. It is quite possible that for large distances of electrode

spacing (multiple centimeter range), such as tested in the other two studies, proton transfer would begin to limit the anodic or cathodic reactions (Cheng and Logan, 2011; Liu et al., 2005). It is also possible that for small distances (< 1 mm), decreasing spacing further would make proton transfer significantly easier. The second aspect is that the media used in our study contained phosphate buffer. It could be that for solutions with very low solution conductivity the electrode spacing would influence performance. Liu et al., 2005 did not use phosphate buffer, but Cheng and Logan, 2011 did use phosphate buffer solution (100 mM), so this aspect is not likely to be the crucial difference in study design. The third aspect of our experimental setup is that the liquid in the region between the electrodes had access to the liquid outside of that region and the freedom to move, since there was neither a cloth separator nor a membrane between them. Low speed and localized water motion could have been present in this region due to processes such as natural convection or small vibrations of the experimental setup, which could have had a large influence on the mixing of chemical species such as protons and proton-carriers. If fluid motions caused the transport of protons to be quick and easy in the region between the outside of the anode biofilm and the cathode surface, or if proton transport in this region is never a problem, then this would cause electrode spacing to have little effect on performance. In neither of the other two studies were separators used. The reason for a different observed effect of electrode spacing is therefore most likely related to the range tested, so changing electrode spacing within the range of 4 to 9 mm is expected to have little or no effect on performance.

It is well-studied that increasing the buffer concentration improves the performance of MECs (Call and Logan, 2008; Sleutels et al., 2009b). Our study found that increasing buffer concentration also improves the performance under the non-shaking condition, although the benefit of additional buffer appeared to be lessening around 200 mM (Fig. 2.1). Additionally, the

current density was found to dramatically decrease with buffer concentrations of 300 mM (not shown), which indicates that high concentration of phosphate buffer solution may chemically inhibit the anode biofilm. The addition of buffer, at non-inhibitory levels, is understood to facilitate proton transport (Fan et al., 2007). Fan et al. (2007) used two equations to demonstrate that diffusion and electric migration of the protons themselves were insufficient to account for rates of proton transport, which were observed as electrical current through the external circuit. This remains true for the MECs tested in this study, but, unlike the study by Fan et al. (2007), the diffusion of the buffer species, as proton carriers, was not found to be sufficiently high to meet observed values. A current density of 35 A/m^2 (total current: 53 mA) was achieved using non-shaking MECs in this study, whereas diffusion of $H_2PO_4^-$ (concentration: 200 mM) across an electrode spacing of 7 mm accounts for only about 4 mA. This suggests that diffusion of buffer species was not the main mechanism of proton transport within the MECs tested and that significant fluid motion may have been present within the MECs, even in the non-shaking setup, since this would increase proton transport.

The influence of changing the mixing conditions was studied by operating the MECs on a shake plate. Shaking the MECs at 90 rpm improved the current density by a similar magnitude as doubling the buffer concentration of the fluid. Mixing by shaking offered a larger improvement in current density when a lower buffer concentration was used. However, this trend may have been exaggerated by the MEC performance being overly-limited by the anode at 200 mM buffer concentration, as shown in the subsequent internal resistance analysis. Fluid motion between the electrodes may improve proton transfer, which was found, using EIS, to be the “dominant resistance” in hydrogen production in a two-chamber MEC (P. Borole and J. Lewis, 2017). This means that addressing fluid mixing conditions likely will be useful for MECs operating with real

waste streams, as these typically have lower buffering capacities and conductivities (~ 1 mS/cm, compared to 7.5 mS/cm for 50mM phosphate buffer) (Call and Logan, 2008; Rozendal et al., 2008).

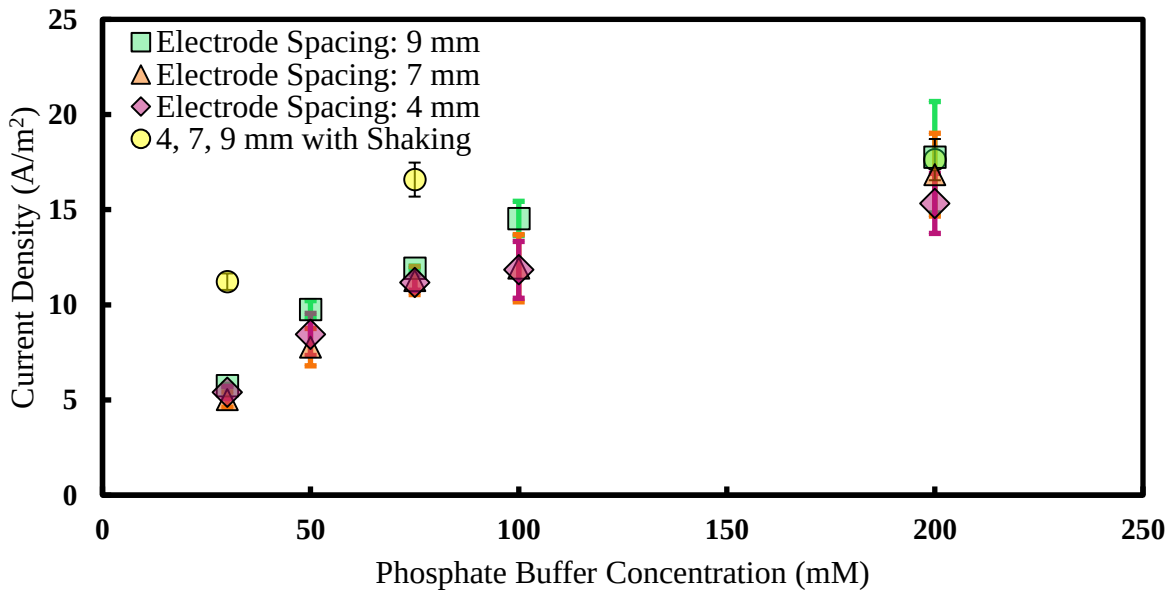

Figure 2.1: MECs operated with differing electrode spacing, buffer concentration, and mixing condition (Input Voltage: 0.8 V ; Error bars: +/- 2*SE ; n = 7: 30, 75, 100 mM buffer concentration, n = 6: 50, 200 mM buffer concentration)

2.3.2 Investigating Performance-Limiting Electrode

By testing the MECs with varying anode to cathode surface area ratio, the anode was found to limit overall performance more than the cathode. Stacking multiple pieces of cloth with anodic biofilm improved performance very significantly, whereas adding a second piece of cloth to the cathode did not improve performance to a great extent, as shown in Figure 2.2. Doubling

the anode surface area increased the current density of the cathode by about 76% compared to the ideal increase of 100%. Tripling the anode surface area increased it by about 150%, from 18 A/m^2 to 46 A/m^2 (with shaking, data not shown), compared to an ideal value of 200%, which would be achieved if current density was completely limited by the anode surface area. Current density for MECs with a 3:1 anode to cathode ratio and with mixing by shaking was indistinguishable from the 4:1 anode to cathode ratio with shaking shown in Figure 2.2.

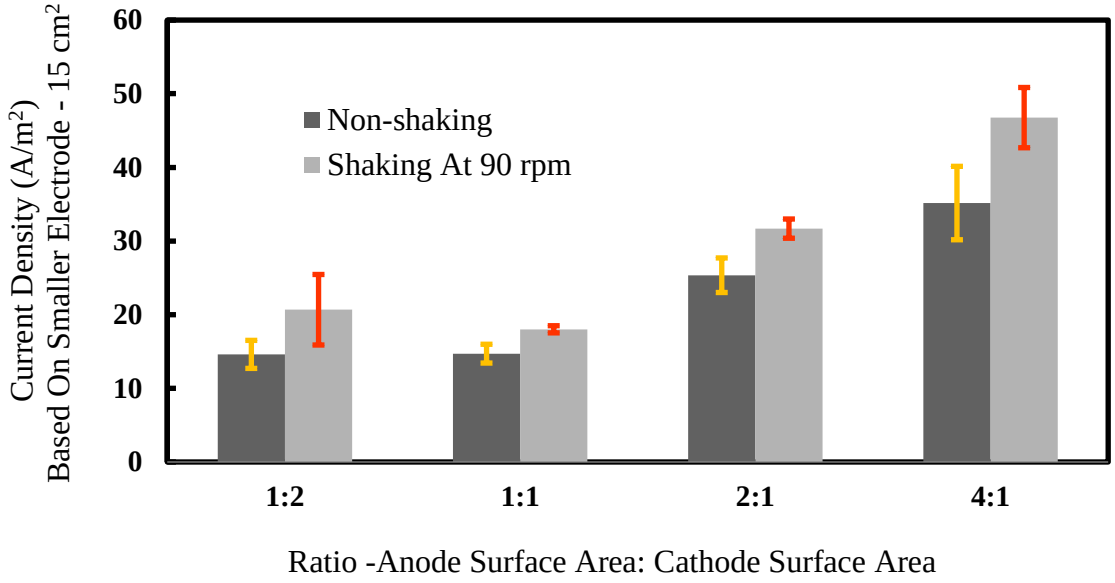

Figure 2.2: Current density based on smaller electrode for MECs with varied anode to cathode ratios; Input voltage: 1.0 V; Error bars: +/- 2*SE (n = 4); Buffer Concentration: 200 mM

The effect of mixing was also tested while varying the electrode ratios, in order to see whether mixing would have a greater alleviating effect on mass-transfer resistance at higher reaction rates (measured as higher current). In Figure 2.2, the increase of current density for the MECs with quadruple the surface area in the anode (4:1) was 33% with shaking, compared to an increase of 23% for the MECs with lower ratios (1:1 and 2:1), which supported this prediction.

2.3.3 Relationship Between H_2-Production and Current Density

Consumption of produced H_2 by microbes has been shown to be an issue in single-chamber MECs. Methanogens were previously found to be the dominant hydrogen consumers (Lee and Rittmann, 2010). However, recent studies have found that homoacetogens can also thrive by producing acetate from H_2 and CO_2 (Parameswaran et al., 2011; Xafenias and Mapelli, 2014). A typical batch experiment in our study (Fig. 2.3A) demonstrates that acetate concentration remained high, while the H_2–production was low and leveled off. H_2-consumption by homoacetogens was hypothesized to be the cause of this batch behavior, which leads to the overestimation of H_2 production based on measured current, as current density remained high during a typical batch (Fig. 2.3B). The measure of how much H_2 is produced relative to the amount expected based on the current is the cathodic H_2 recovery. The cathodic H_2 recovery decreased from about 0.4 to about 0 throughout the batch, indicating that the majority of the hydrogen produced at the cathode was likely being consumed (Fig. 2.3B). In order to verify that current density was an appropriate measure to assess the MEC performance, a method using chloroform (unpublished work) as specific homoactogenesis inhibitor, was applied in this study. With the addition of inhibitor (0.02% v/v), the acetate concentration decreased constantly throughout the batch, due to the impairment of acetate synthesis from homoacetogenic hydrogen consumption (Fig. 2.3A). At the same time, the volume of H_2 that was produced increased dramatically. Correspondingly, the cathodic hydrogen recovery changed to about 85% consistently through the batch (Fig. 2.3B). The current density did not change in a noticeable way with the addition of the chemical inhibitor. High and stable cathodic hydrogen recoveries after treatment reaffirm that current density is a good surrogate measurement for the H_2 gas production rate that an MEC can achieve following the elimination of H_2-consumption.

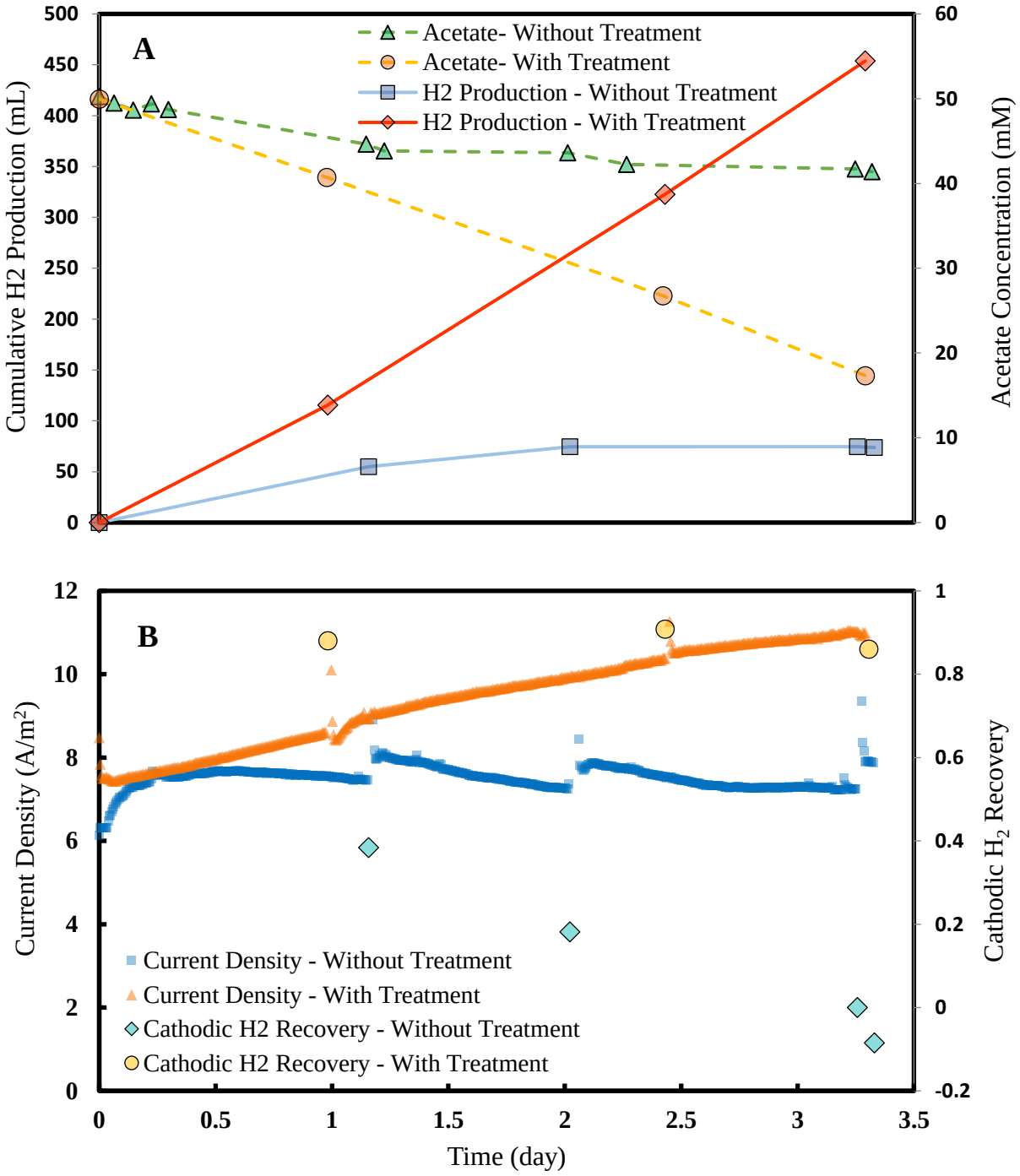

Figure 2.3: Representative batch behavior for MEC without and with treatment to prevent homoacetogenic H_2-consumption (A) Acetate concentration and H_2-Production (B) Current density and cathodic hydrogen recovery

An average H_2-production rate of 3.7 L/L/d and a current density of 47 A/m^2 were achieved for two MECs operated concurrently. The anode to cathode surface area ratio was 4:1, and the MECs were operated at an input voltage of 1.0 V, with the shaking mixing condition. The H_2 yield was 3.4 mol-H_2/mol-acetate, compared to the ideal value of 4 mol-H_2/mol-acetate. The cathodic H_2 recovery was 75%, and the energy yield relative to electrical input was 110%.

2.3.4 Dissecting Internal Resistance

Experiments that involved operating MECs at varying input voltages were completed in order to identify the internal resistance of each, and to divide it into three portions, relating to the anode surface area, the cathode surface area, and the solution buffer concentration. The observed relationship between the applied voltage and the measured current (Fig. 2.4) agreed well with the resistance model (Equation 2.7). The internal resistance analysis used in this study (Equation 2.7) is related to one developed for MFCs (Fan et al., 2008), and it was modified to account for the mixing condition and to be used with MECs. All of the MECs that were operated in a given mixing condition experienced a linear range with the same linearly-predicted voltage for zero-current. The least-squares analyses for both shaking and non-shaking conditions found the values for four parameters. Three of these related to the design variables that were modified (anode and cathode surface area, and buffer concentration), and the final value was the linearly-predicted voltage for zero-current. The parameters corresponding to the anode, cathode, and solution provide insight on appropriate design settings in which the resistance of each of these three components will be balanced, so that the MEC is not overly limited by one component.

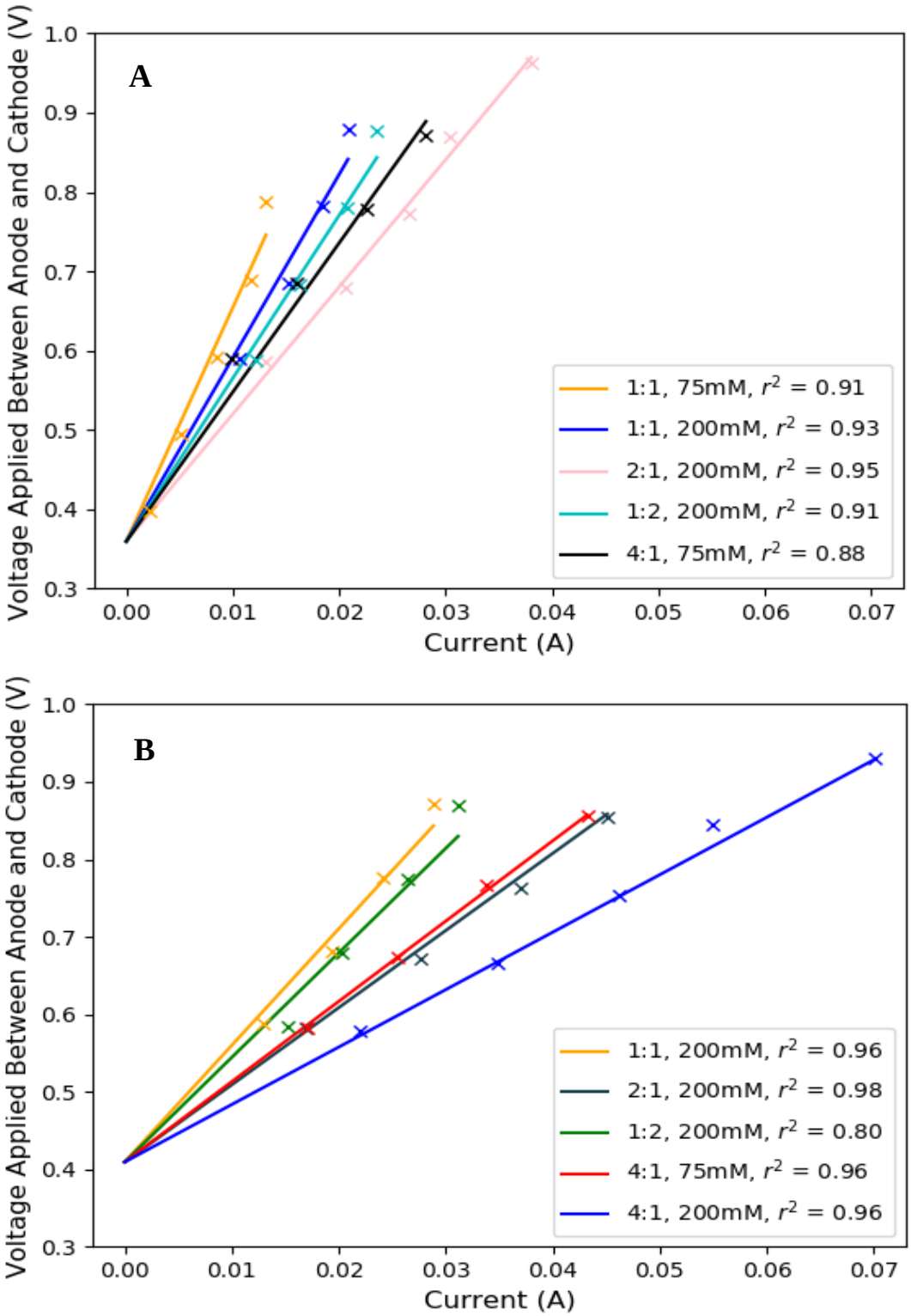

Figure 2.4: Voltage required for the a range of electrical currents for five MECs with various anode to cathode surface area ratios, and buffer concentrations (A) Tests with low mixing condition: non-shaking (B) Tests with high mixing condition: shaking

Table 2.1: Internal resistance model results for both mixing conditions: anode, cathode, and solution resistivities; voltage for zero-current; design and expected performance of balanced internal resistance MEC (PBS: Phosphate Buffer Solution)

Term [units]	**Non-Shaking**	**Shaking**
r_{An} [Ω cm^2]	210	150
r_{Cat} [Ω cm^2]	77	47
α_{Sol} [Ω cm^2 M]	11 200 mM PBS → 57 Ω cm^2 75 mM PBS → 150 Ω m^2	5.3 200 mM PBS → 27 Ω cm^2 75 mM PBS → 71 Ω m^2
$V_{Zero-Current}$ [V]	0.36	0.41
Balanced Anode : Cathode Surface Area Ratio	3 : 1	3.5 : 1
Balanced Buffer Concentration [mM]	150	110
Input Voltage to Achieve 30 A/m^2 [V]	1.03	0.82

The results suggest that a MEC with an anode : cathode surface area ratio of about 3.5 : 1 , with shaking, and a phosphate buffer concentration of about 120 mM will have well-balanced internal resistance. This agrees well with the findings that a MEC with an anode to cathode surface area ratio of 3 : 1 had a higher current density than one with a 2 : 1 ratio, but that current density was indistinguishable from a MEC with a 4 : 1 ratio (with shaking; input voltage: 1.0 V; phosphate buffer concentration: 200 mM). A MEC's performance will be expected to be limited by the solution if waste streams with lower solution conductivity than that of 120 mM phosphate buffer are used, or if they are used in a MEC with little fluid motion. MECs with the same anode community and cathode catalyst, and with a surface area of carbon cloth in the anode less than triple that of the cathode, will have a higher anode resistance than cathode resistance. On the other hand, if the surface area of the anode is more than quadruple that of the cathode, then it will be 'cathode-limited', meaning that the cathode resistance will be higher.

When the resistivity values were compared to those obtained by Fan et al., 2008 for MFCs, the same design decisions were found to affect overall performance differently. Whereas in this study the anode limited current density more than the cathode (resistivities of 210 and 77 Ω m^2, respectively), in the MFC study the cathode was more limiting than the anode (resistivities of 280 and 32 Ω m^2). Although the anodes were very similar between the two studies, the cathode had a different design and supported a different chemical reaction for two bioelectrochemical devices. Therefore, the resistivity found for the anode was likely related to how much it was limiting performance as compared to the cathode. Secondly, the solution resistance found by Fan et al., 2008 was 57 Ω m^2 M, compared to 11 Ω m^2 M, found in this study. This higher value is likely due to the differences in both the electrode spacing and cathodic reaction. In the MFC study the anode and cathode were separated by about 4 cm, as compared to about 1 cm, so proton transport between the electrodes could have limited performance, causing a higher solution resistance (Fan et al., 2008). The different cathodic reactions between the two bioelectrochemical devices changes the impact on performance that comes with increasing the solution buffer concentration.

Improving mixing by shaking the MECs decreased the resistivities of the anode, cathode, and solution by about 28%, 40%, and 53%, respectively (Table 2.1). This signifies that the ‘solution resistance’ (the resistance that is decreased by increasing the buffer concentration of the solution) was most affected by mixing, but the resistances associated with each of the electrode surface areas were also affected. The values of the different resistances found with the design decision internal resistance method are not the same as those obtained through EIS. For example, the ‘anode resistance’ found with EIS is the estimated charge transfer resistance (and sometimes also the mass transfer resistance) of the anodic reactions, whereas the ‘anode resistance’ in this

study is the portion of the overall MEC resistance that decreases with increasing anode surface area. So, the electrode resistances might be affected by shaking because processes such as proton transport and substrate consumption are influenced by local chemical concentrations at electrode-fluid interfaces.

EIS was performed on MECs with two different electrode spacings (Appendix A, Fig. 2.9). The values of ohmic/ionic solution resistance found with EIS were compared with the values of 'solution resistance' found using the design decision internal resistance method. Ionic resistance is the resistance of a solution to the movement of ions through it, which is how current moves through the solution in electrolytic cells. Somewhat differently, the solution resistance found in this study is the MEC resistance that decreases with increasing buffer concentration in the solution and with larger cross-sectional surface areas between the electrodes. The ionic resistance values were multiplied by the surface area of the electrode (15 cm^2) to calculate resistivity values. The ionic resistivity values were found to be 50 Ω cm^2 and 67 Ω cm^2 for the MECs with electrode spacings of 7 mm and 9 mm, respectively. These values of ionic resistivity fit well within the range of values found in other studies, especially among the studies with the most similar MECs and operating conditions (Appendix A, Table 2.2). Dividing these values by the electrode spacing demonstrates that ionic resistance increases linearly with the spacing at a rate of about 74 Ω cm^2/cm for the buffer concentration used (75 mM). The ionic resistance is a smaller portion of the MEC's total internal resistance than the portion relating to solution design decisions (resistivity: 150 Ω cm^2). For a MEC operated in a stationary condition, with a 3:1 anode : cathode surface area ratio and 75 mM buffer, the ionic resistance and the design decision solution resistance represent approximately 17% and 51%, respectively, of the total resistance of the MEC.

This regression analysis was developed using observed data from MECs that were operated with at least four different input voltages, so that the linear relationship between input voltage and current could be observed and compared to model results. For input voltages greater than the ones shown in Figure 2.4, the current produced began to level-off. One MEC in each mixing condition displayed linear behavior up to 1.0 V. Separate MEC batch trials, in which they were not operated across a full range of input voltages, were used to verify that the model results were not applicable only to the 'model training' data in Figure 2.5. The performance (current) predicted for the 'model testing' batches is similar to the observed current, for both MECs under shaking and non-mixing-condition (Fig. 2.5). The internal resistance method was therefore useful for predicting performance for MECs designed according to our study and operated within the range of operational conditions used (30 mM ≤ [Phosphate Buffer Concentration] ≤ 200 mM, 1 : 2 ≤ [Anode : Cathode Ratio] ≤ 4 : 1, 0.6 V ≤ [Input Voltage] ≤ 1.0 V).

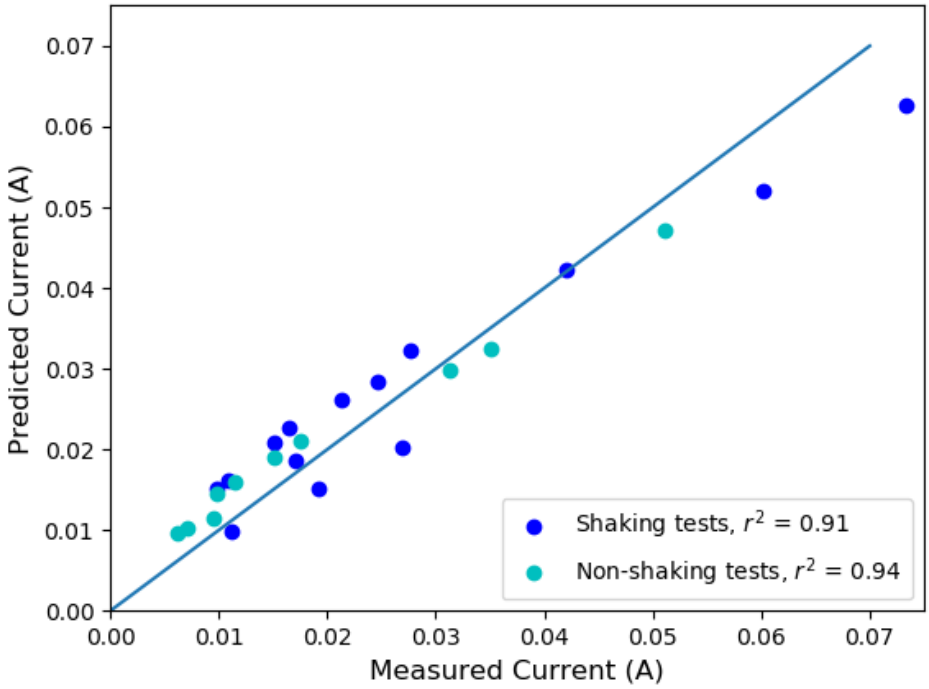

Figure 2.5: Current of various MECs not used to train the internal resistance model compared to the current predicted based on their design settings and operational conditions

2.3.5 Predicting Performance of Other Studies

The parameters found from the internal resistance analysis were used to predict the current density of two different single chamber membrane-less MECs from previous studies, as shown in Figure 2.6. These studies were chosen because they had similar designs to the ones tested in this study and they were both tested at a range of input voltages. In addition, both of these studies focused on the effect of electrode configurations on performance, which is a focus of this study. The MEC from each study that was most similar to the ones used in this study was chosen. In those studies, both MECs were tested within the range of input voltages that were found to produce a linear response, and that linear range overlapped with the linear range found in our study (0.6 - 1.0 V). Both MECs had carbon cloth based cathodes and the anodes were graphite brush and graphite felt. It was necessary to relate the anodes to an approximately equivalent projected surface area of layered carbon cloth, in order to predict current density using our study results. The carbon cloth used in this study was approximately one millimeter thick (0.9 mm), so each millimeter of depth in the graphite brush and graphite felt anodes was approximated as a layer of carbon cloth. As an example, the equivalent surface area of a 5 mm thick piece of graphite felt anode used by Liang et al., 2011 was five times the length (4 cm) multiplied by the width (3.5 cm). Additionally, the cathodes were loaded with platinum (Pt) catalyst, rather than MoP catalyst, but this catalyst performed comparably well in MECs (unpublished data), so the cathode surface area was not modified. The values adapted from those studies that were used in our internal resistance method are detailed in Appendix A (Table 2.3). The data reported by Liang et al., 2011 was found to fit more closely to the performance predicted with a ‘high mixing condition’, whereas the data reported by Cheng and Logan, 2011 fit more closely when a ‘low mixing condition’ was used. It is argued that the high and low

mixing conditions provide approximate bounds on the performance that one can predict for a MEC designed with specific settings.

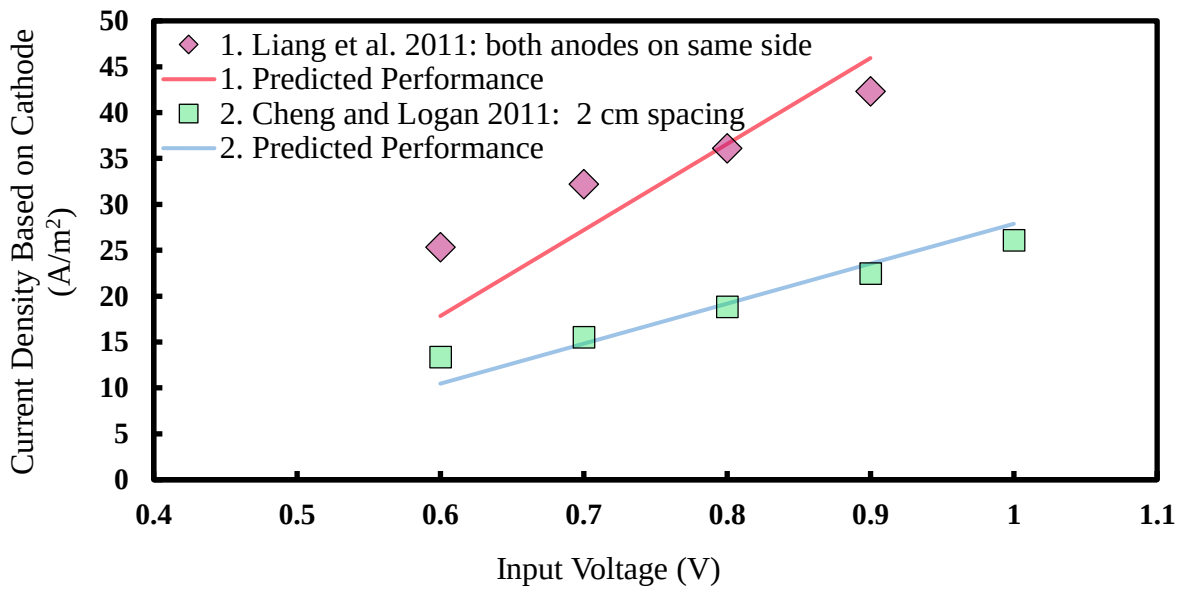

Figure 2.6: Subsection of the observed data from two different studies compared to the performance predicted using the design decision internal resistance model

The MEC operated by Liang et al., 2011 was estimated to be limited about equally by solution resistance and cathode resistance (50 and 44% of the total internal resistance, respectively). Somewhat differently, the MEC operated by Cheng and Logan was limited most by solution resistance (50% of total internal resistance, compared to 34% and 17% for cathode and anode resistance, respectively).

2.4 IMPLICATIONS

This study clarifies the design settings and priorities that will enable high performance for a membrane-less single-chamber MEC with carbon cloth electrodes. The findings are:

- Impact on MEC performance: Input Voltage, Electrode Surface Area Ratio > Buffer Concentration, Mixing Condition > Electrode Spacing
- Fluid motion improves MEC performance as alternative to chemical addition to influent
- Optimal anode surface area: cathode surface area ratio of ~3.5:1
- Layering carbon cloth works well to increase anode surface area

An understanding of the influence of design decisions on internal resistance was developed to support these findings. This internal resistance model also provides a reasonably accurate prediction of the current of two other MECs that were designed with similar materials. It follows that the method for equating different types of carbon-based anodes with carbon cloth may be suitable. This approximation is that each millimeter of depth of a carbon-based anode is equivalent to a layer of carbon cloth (Appendix A, Table 2.3). This work also gives insight on which design decision is most limiting overall MEC performance for a given design (eg. anode surface area or mixing condition). Therefore, a low-internal resistance MEC can be designed according to the recommendations above. Once it is constructed and tested, it can be determined how much fluid mixing condition is likely limiting overall performance. Additionally, this relation of design with performance can be used to validate upcoming mechanistic models of single chamber membrane-less MECs. In new models of MEC microbial and electrochemical dynamics, the same design factors can be varied and the effect on current density can be compared with those found in this study.

2.5 REFERENCES

Barbosa, S.G., Peixoto, L., Soares, O.S.G.P., Pereira, M.F.R., Heijne, A.T., Kuntke, P., Alves, M.M., Pereira, M.A., 2018. Influence of carbon anode properties on performance and microbiome of Microbial Electrolysis Cells operated on urine. Electrochimica Acta 267, 122–132. https://doi.org/10.1016/j.electacta.2018.02.083

Bond, D.R., Lovley, D.R., 2003. Electricity Production by Geobacter sulfurreducens Attached to Electrodes. Appl. Environ. Microbiol. 69, 1548–1555. https://doi.org/10.1128/AEM.69.3.1548-1555.2003

Call, D., Logan, B.E., 2008. Hydrogen Production in a Single Chamber Microbial Electrolysis Cell Lacking a Membrane. Environ. Sci. Technol. 42, 3401–3406. https://doi.org/10.1021/es8001822

Cheng, S., Logan, B.E., 2011. High hydrogen production rate of microbial electrolysis cell (MEC) with reduced electrode spacing. Bioresour. Technol. 102, 3571–3574. https://doi.org/10.1016/j.biortech.2010.10.025

Dominguez-Benetton, X., Sevda, S., Vanbroekhoven, K., Pant, D., 2012. The accurate use of impedance analysis for the study of microbial electrochemical systems. Chem. Soc. Rev. 41, 7228–7246. https://doi.org/10.1039/C2CS35026B

Dudley, H.J., Lu, L., Ren, Z.J., Bortz, D.M., 2018. Sensitivity and Bifurcation Analysis of a DAE Model for a Microbial Electrolysis Cell. ArXiv180206326 Math Q-Bio.

Fan, Y., Hu, H., Liu, H., 2007. Sustainable Power Generation in Microbial Fuel Cells Using Bicarbonate Buffer and Proton Transfer Mechanisms. Environ. Sci. Technol. 41, 8154–8158. https://doi.org/10.1021/es071739c

Fan, Y., Sharbrough, E., Liu, H., 2008. Quantification of the Internal Resistance Distribution of Microbial Fuel Cells. Environ. Sci. Technol. 42, 8101–8107. https://doi.org/10.1021/es801229j

Gadkari, S., Gu, S., Sadhukhan, J., 2018. Towards automated design of bioelectrochemical systems: A comprehensive review of mathematical models. Chem. Eng. J. 343, 303–316. https://doi.org/10.1016/j.cej.2018.03.005

Gil-Carrera, L., Mehta, P., Escapa, A., Morán, A., García, V., Guiot, S.R., Tartakovsky, B., 2011. Optimizing the electrode size and arrangement in a microbial electrolysis cell. Bioresour. Technol. 102, 9593–9598. https://doi.org/10.1016/j.biortech.2011.08.026

Guo, K., Prévoteau, A., Rabaey, K., 2017. A novel tubular microbial electrolysis cell for high rate hydrogen production. J. Power Sources 356, 484–490. https://doi.org/10.1016/j.jpowsour.2017.03.029

Hu, H., Fan, Y., Liu, H., 2008. Hydrogen production using single-chamber membrane-free microbial electrolysis cells. Water Res. 42, 4172–4178. https://doi.org/10.1016/j.watres.2008.06.015

Kadier, A., Kalil, M.S., Abdeshahian, P., Chandrasekhar, K., Mohamed, A., Azman, N.F., Logroño, W., Simayi, Y., Hamid, A.A., 2016. Recent advances and emerging challenges in microbial electrolysis cells (MECs) for microbial production of hydrogen and value-added chemicals. Renew. Sustain. Energy Rev. 61, 501–525. https://doi.org/10.1016/j.rser.2016.04.017

Ki, D., Popat, S.C., Torres, C.I., 2016. Reduced overpotentials in microbial electrolysis cells through improved design, operation, and electrochemical characterization. Chem. Eng. J. 287, 181–188. https://doi.org/10.1016/j.cej.2015.11.022

Lee, H.-S., Rittmann, B.E., 2010. Significance of Biological Hydrogen Oxidation in a Continuous Single-Chamber Microbial Electrolysis Cell. Environ. Sci. Technol. 44, 948–954. https://doi.org/10.1021/es9025358

Liang, D.-W., Peng, S.-K., Lu, S.-F., Liu, Y.-Y., Lan, F., Xiang, Y., 2011. Enhancement of hydrogen production in a single chamber microbial electrolysis cell through anode arrangement optimization. Bioresour. Technol. 102, 10881–10885. https://doi.org/10.1016/j.biortech.2011.09.028

Liu, H., Cheng, S., Logan, B.E., 2005. Power Generation in Fed-Batch Microbial Fuel Cells as a Function of Ionic Strength, Temperature, and Reactor Configuration. Environ. Sci. Technol. 39, 5488–5493. https://doi.org/10.1021/es050316c

Liu, H., Logan, B.E., 2004. Electricity Generation Using an Air-Cathode Single Chamber Microbial Fuel Cell in the Presence and Absence of a Proton Exchange Membrane. Environ. Sci. Technol. 38, 4040–4046. https://doi.org/10.1021/es0499344

Liu, J., Zhang, F., He, W., Yang, W., Feng, Y., Logan, B.E., 2014. A microbial fluidized electrode electrolysis cell (MFEEC) for enhanced hydrogen production. J. Power Sources 271, 530–533. https://doi.org/10.1016/j.jpowsour.2014.08.042

Logan, B.E., Call, D., Cheng, S., Hamelers, H.V.M., Sleutels, T.H.J.A., Jeremiasse, A.W., Rozendal, R.A., 2008. Microbial Electrolysis Cells for High Yield Hydrogen Gas Production from Organic Matter. Environ. Sci. Technol. 42, 8630–8640. https://doi.org/10.1021/es801553z

Parameswaran, P., Torres, C.I., Lee, H.-S., Rittmann, B.E., Krajmalnik-Brown, R., 2011. Hydrogen consumption in microbial electrochemical systems (MXCs): The role of homo-acetogenic bacteria. Bioresour. Technol., Special Issue: Biofuels - II: Algal Biofuels and Microbial Fuel Cells 102, 263–271. https://doi.org/10.1016/j.biortech.2010.03.133

P. Borole, A., J. Lewis, A., 2017. Proton transfer in microbial electrolysis cells. Sustain. Energy Fuels 1, 725–736. https://doi.org/10.1039/C7SE00034K

Rozendal, R.A., Hamelers, H.V.M., Rabaey, K., Keller, J., Buisman, C.J.N., 2008. Towards practical implementation of bioelectrochemical wastewater treatment. Trends Biotechnol. 26, 450–459. https://doi.org/10.1016/j.tibtech.2008.04.008

Sedaqatvand, R., Nasr Esfahany, M., Behzad, T., Mohseni, M., Mardanpour, M.M., 2013. Parameter estimation and characterization of a single-chamber microbial fuel cell for dairy wastewater treatment. Bioresour. Technol. 146, 247–253. https://doi.org/10.1016/j.biortech.2013.07.054

Sleutels, T.H.J.A., Hamelers, H.V.M., Rozendal, R.A., Buisman, C.J.N., 2009a. Ion transport resistance in Microbial Electrolysis Cells with anion and cation exchange membranes. Int. J. Hydrog. Energy 34, 3612–3620. https://doi.org/10.1016/j.ijhydene.2009.03.004

Sleutels, T.H.J.A., Heijne, A.T., Buisman, C.J.N., Hamelers, H.V.M., 2013. Steady-state performance and chemical efficiency of Microbial Electrolysis Cells. Int. J. Hydrog. Energy 38, 7201–7208. https://doi.org/10.1016/j.ijhydene.2013.04.067

Sleutels, T.H.J.A., Lodder, R., Hamelers, H.V.M., Buisman, C.J.N., 2009b. Improved performance of porous bio-anodes in microbial electrolysis cells by enhancing mass and charge transport. Int. J. Hydrog. Energy 34, 9655–9661. https://doi.org/10.1016/j.ijhydene.2009.09.089

Tartakovsky, B., Manuel, M.-F., Wang, H., Guiot, S.R., 2009. High rate membrane-less microbial electrolysis cell for continuous hydrogen production. Int. J. Hydrog. Energy 34, 672–677. https://doi.org/10.1016/j.ijhydene.2008.11.003

Tartakovsky, B., Mehta, P., Santoyo, G., Guiot, S.R., 2011. Maximizing hydrogen production in a microbial electrolysis cell by real-time optimization of applied voltage. Int. J. Hydrog. Energy, International Conference on Hydrogen Production (ICH2P)-2010 36, 10557–10564. https://doi.org/10.1016/j.ijhydene.2011.05.162

Xafenias, N., Mapelli, V., 2014. Performance and bacterial enrichment of bioelectrochemical systems during methane and acetate production. Int. J. Hydrog. Energy 39, 21864–21875. https://doi.org/10.1016/j.ijhydene.2014.05.038

Chapter 3: Scaled-up MEC Reactor Design and Evaluation

3.1 INTRODUCTION

In the last ten or so years Microbial Electrolysis Cells (MECs) have been rapidly improved as devices for producing H_2 gas. H_2 is a desirable clean-burning fuel and is also useful for synthesizing other products (Ramachandran and Menon, 1998). The key strength of MECs for producing H_2 is that microorganisms harvest energy within wastewater, in the form of dissolved organic material, as part of the energy required for the process. In this way, MECs are similar to dark fermentation reactors, but the advantage of MECs are that they can utilize volatile fatty acids (VFAs) and other organic compounds, whereas dark fermentation requires fermentable sugars. By oxidizing the organic material further MECs are able to produce higher amounts of H_2 for the same amount of sugars in a waste stream, up to 8.55 mol-H_2/mol-glucose versus about 2-3 mol -H_2/mol-glucose for dark fermentation systems (Cheng and Logan, 2007; Hawkes et al., 2007). MECs also work on some waste streams, such as waste activated sludge with low amounts of carbohydrates (Lu et al., 2012). The trade-off inherent in MEC technology is that it requires input energy in the form of low voltage electricity (0.3 – 1 V, but typically 0.7 – 1 V) in order to make the evolution of H_2 favorable (Kadier et al., 2016). Secondly, H_2-production rates are frequently lower than dark fermentation reactors, though of the same order of magnitude (Cheng and Logan, 2007). However, for certain applications MEC technology is likely to be the favored technology for wastewater, due to their high fuel yield and oxidation of organic contaminants (Lu et al., 2012).

In the near-term the main draw for implementing these systems will likely be situations where MECs compare favorably with other methods, such as aerobic activated sludge and anaerobic digestion, for lowering the strength of wastewater while recovering energy. However, from a wider perspective, their suitability for fitting within grids or micro grids to store electrical energy as H_2, or for being large-scale fuel sources and wastewater treatment devices are topics of active investigation (Escapa et al., 2016).

MECs studied in the past have been either ‘single-chamber’ or ‘two-chamber’. Single-chamber MECs have both the anode and the cathode within the solution, whereas the two-chamber MECs have the anode in the wastewater to be treated and the cathode in another solution that is separated by a membrane. Two-chamber MECs have one main advantage, which is that they can produce higher-purity H_2 (less CO_2) and have a decreased risk of H_2-consumption by microbes (Guo et al., 2017). However, the disadvantages include performance-lowering pH gradients and ohmic resistance, caused by the membrane (Guo et al., 2017). For small-scale MECs both options are suitable, but for large-scale MEC reactors, single-chamber designs will likely be highly preferable, as long as H_2-consumption can be suitably controlled. This is because of design and materials factors. Two-chamber designs require that the anode and cathode chambers be sealed off from each other with a membrane, and this will be costly for large MEC reactors. The membrane itself will be a barrier to scale-up, since it is difficult to develop a cheap membrane that can also seal well. The membrane must also resist biofouling while being selective-enough to restrict bacteria from entering the cathode chamber, which occurred with the reactor operated by Coterill et al., negating the benefits of a two-chamber design (Cotterill S. E. et al., 2017).

So far there have been a handful of papers published on moderately-sized laboratory scale reactors (0.1– 1 L) and a couple on large laboratory scale reactors (1-10 L), but surprisingly few on reactors with volumes between 10 and 100 L. There have also been a few designs of pilot-scale reactors published, with volumes of about 100 L and 1000 L, that have been tested on-site for wastewater treatment (Cotterill S. E. et al., 2017; Cusick et al., 2011). The performance for MEC reactors larger than 1 L in volume has generally been low, in terms of both H_2-production rates and current density (Appendix B, Table 3.1). H_2-production rates are mostly below 1 L/L-reactor/day, likely due to a combination of H_2-consumption and limitations to the amount of current possible with the reactor design. Many of the reactors transitioned to producing mostly methane, and while methane is also a useful fuel, MECs are not currently producing it at a level to compete with high-performance anaerobic digesters (Cusick et al., 2011; Hou et al., 2015). Two reactors (0.855 L and 1 L in volume) with notably high current densities (8.14 A/m^2 and 27.8 +/- 0.10 A/m^2, by cathode surface area) were operated in ways that encouraged fluid mixing throughout the reactor (Gil-Carrera et al., 2013; Guo et al., 2017). The highest performing reactor of the two was a two-chamber reactor. Operated using acetate as substrate, this reactor exhibited a high H_2-production rate (7.1 +/- 0.01 L/L/d), but its suitability for scale-up by two or three orders of magnitude is uncertain due to its two-chamber design (Guo et al., 2017). Additionally, this reactor used a cathode that contained precious metals (platinum-coated titanium mesh), which is not practical for use in an affordable scaled-up MEC reactor. The 0.855 L reactor operated by Gil-Carrera et al. had a good H_2-production rate of 2.54 L/L/d, likely in part because it has a gas diffusion cathode on the wall of the reactor that releases H_2 to be collected (Gil-Carrera et al., 2013). This decreases the amount of H_2 that is consumed within the reactor, but it may be difficult to scale, since larger reactors will have lower wall surface area

to volume ratios. Alternatively, many smaller reactors could take the place of one larger reactor, but this would likely have a high operational cost and complexity, and might have a larger footprint. Thus, there is a need for new single-chamber designs that are more amenable to scaling and have high production rates.

In this study, we designed a 10 L single-chamber reactor with a height to width ratio of about 11:1 and a rectangular cross section. The rectangular cross-section of this design allowed for 5 electrode pairs to be added to the reactor. Further scale-up would involve simply extending the width-dimension of the reactor and adding additional electrode pairs. The 11:1 height to width ratio enables the solution to move up at a higher speed through the electrodes during recirculuation than it would for a more cube-shaped reactor. The reactor was evaluated using synthetic waste water (acetate as substrate), so that performance of the reactor could be assessed without the additional complications of waste water, and so that it can be directly compared with small-scale tests in the literature.

3.2 MATERIALS AND METHODS

3.2.1 Reactor Design

A MEC reactor was designed and constructed out of acylic plastic (Fig. 3.1).

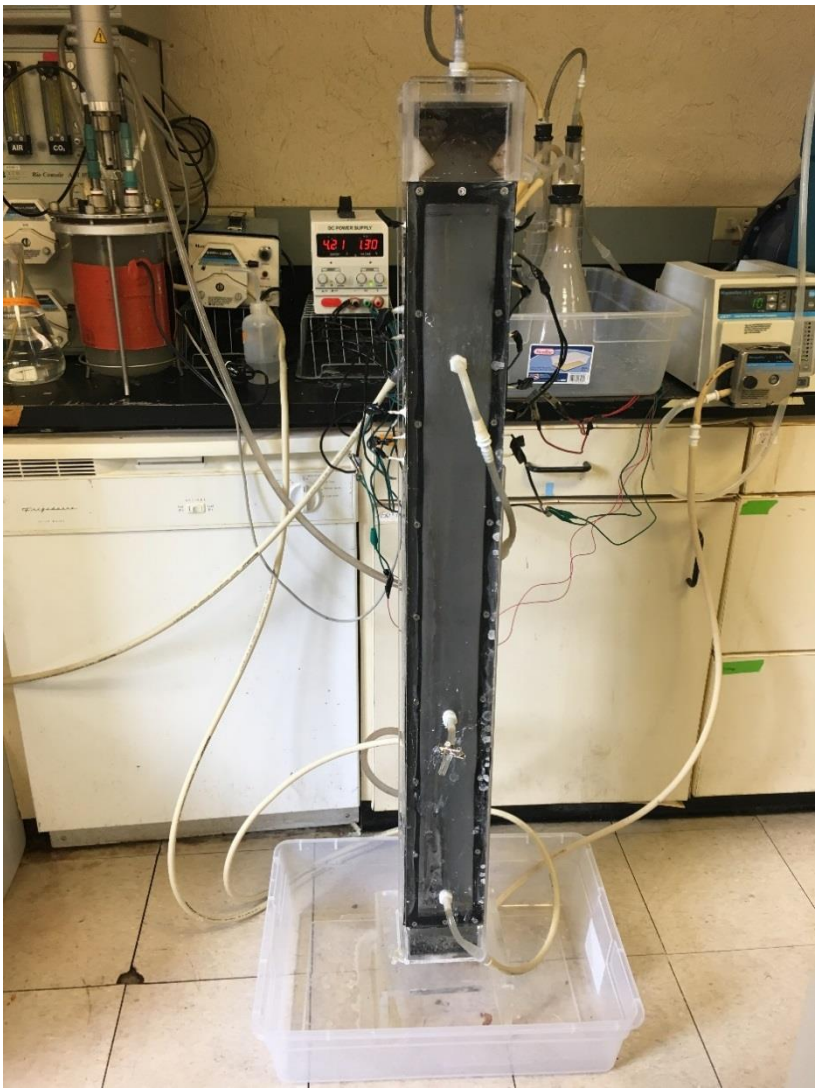

Figure 3.1: Reactor setup showing recirculation tank for heating liquid, pumps, power supply, and liquid-gas separation flask

The electrodes are vertical within the reactor and are about 100 cm tall (Appendix B, Fig. 3.7A). Each cathode consisted of a single piece of carbon cloth (E-Tek, USA) with a projected surface area of 563 cm^2. The carbon cloth was clamped tightly between a folded frame of 316 stainless steel (0.45 mm thick) that was fastened together using nylon screws and nuts. The anodes in both configurations consisted of six sets of three pieces of carbon cloth (each 563 cm^2) for a total surface area of 1.0 m^2. Each set of three pieces of cloth was clamped in the same way as the cathodes, but using a titanium frame (Grade 2, 0.5 mm thick) rather than stainless steel.

3.2.2 Anode Innoculation and Cathode Catalyst

The anode was innoculated with biomass transferred from other MECs operating using acetate and glucose as substrate. The community was originally enriched from local domestic wastewater (Liu and Logan, 2004). The cathode catalyst was a Molybdenum Phosphide (MoP) catalyst developed at Pacific Northwest National Lab (unpublished). The cathode was prepared as follows: (i) the MoP catalyst was mixed with Nafion (5%, Sigma–Aldrich) for 10 h in a ratio of 7 mL Nafion per mg of MoP catalyst to form a solution; (ii) the solution was applied on both sides of the cathode using an airbrush (iii) the cathode was dried at room temperature for 24 h.

3.2.3 Immobilized Fermentative Bacterial Beads

Beads were made by following the method for Acrylic Latex Silicone Beads from Wu et al., except seed sludge was from the Corvallis Wastewater Treatment Plant (Wu et al., 2002). Beads were acclimated in batch mode, using the media from Wu et al. 2002, except mock

lignocellulose hydrolysate was substituted for sucrose. Lignocellulosic hydrolysate was mimicked using the following mixture: 11.7 g/L glucose, 5.12 g/L xylose, 1.5 g/L mannose, 1.0 g/L galactose, and 0.58 g/L arabinose.

3.2.4 Reactor Configurations

The reactor was operated with two different configurations, the 3-cathode configuration (3C – 0.17 m^2 of cathode material) and the 5-cathode configuration (5C– 0.28 m^2 of cathode material). The cathode surface area to volume ratio for the 3C and the 5C configuration were 17 and 28 m^2/m^3, respectively. For the 3C reactor, the anodes and the cathodes were restricted from touching each other in two different ways (Fig. 3.2). One set of anodes was separated from the cathode using J-Cloth (First Brands Corporation, USA). This allowed the set of anodes to be close to the cathode, about 0.9 cm away. A second set of anodes was separated from the cathode by about 1.2 mm, and for this one no separator cloth was used, since it was likely too far of a distance for the anode cloth to physically contact the cathode cloth. The final MEC had one anode separated in the first way, with a narrow distance and using J-Cloth separator, and the second anode separated in the second way, with a wider distance and no separator. For the 5C reactor all of the sets of anodes were separated from the cathodes using a J-Cloth separator and a narrow electrode spacing, except for the the anode to the right of the ‘Right’ cathode (Fig. 3.2B). This rightmost anode set was separated from the cathode by a wider electrode spacing and had no separator cloth. In the 5C configuration 200 mL of fermentative beads were added to a 0.8 L compartment below the MEC electrodes, with a porous plastic piece restricting motion of the beads to the rest of the reactor.

3.2.5 Reactor Operation and Measurement

Influent was pumped continuously into the reactor using a peristaltic pump (MasterFlex 7523-40, Barnant Co.). In the 3C configuration, the influent contained 50 mM acetate as substrate and 100 mM phosphate buffer with the following (per liter): NaH2PO4, 10.2 g; Na2HPO4, 33.8 g; NH4Cl, 0.31 g; KCl, 0.13 g; and mineral (12.5 mL) and vitamin (12.5 mL) solutions as reported (Bond and Lovley, 2003). In the 5C configuration, the influent contained both 50 mM acetate and 2 g/L glucose substrate and 150 mM bicarbonate buffer. The inorganic supplements in the medium were added as described by Wu et al. (Wu et al., 2002). The solution within the reactor was re-circulated through two outlets in the top and two inlets in the bottom (Fig. 3.2). Before returning to the reactor the recirculated liquid entered a heated recirculation tank. The temperature of the liquid in the middle of the MEC reactor was maintained at 32°C. The input voltage was applied between the anodes and cathodes, in parallel, by a DC power supply (Yescom, max current: 10 A). The voltages across 0.1 Ω resistors located between each cathode and the power supply were used to calculate the electrical current. These voltage values were recorded every seven minutes by a data-acquisition system (2700, Keithly, USA). Gas and liquid exited through the top of the reactor, and then it was separated in flask. The gas volume was measured continuously using a drum-type gas meter (Ritter, TG 0.5 Plastic). Gas was sampled from a port on the effluent tube, just above the top of the reactor, and was analyzed using a gas chromatograph (Agilent, 6890N; J&W Scientific, USA) equipped with a thermal conductivity detector and a column (113-3133 CARBONPLT, 30 m x 0.32mm x 3 mm, J&W Scientific, USA) with argon as the carrier gas.

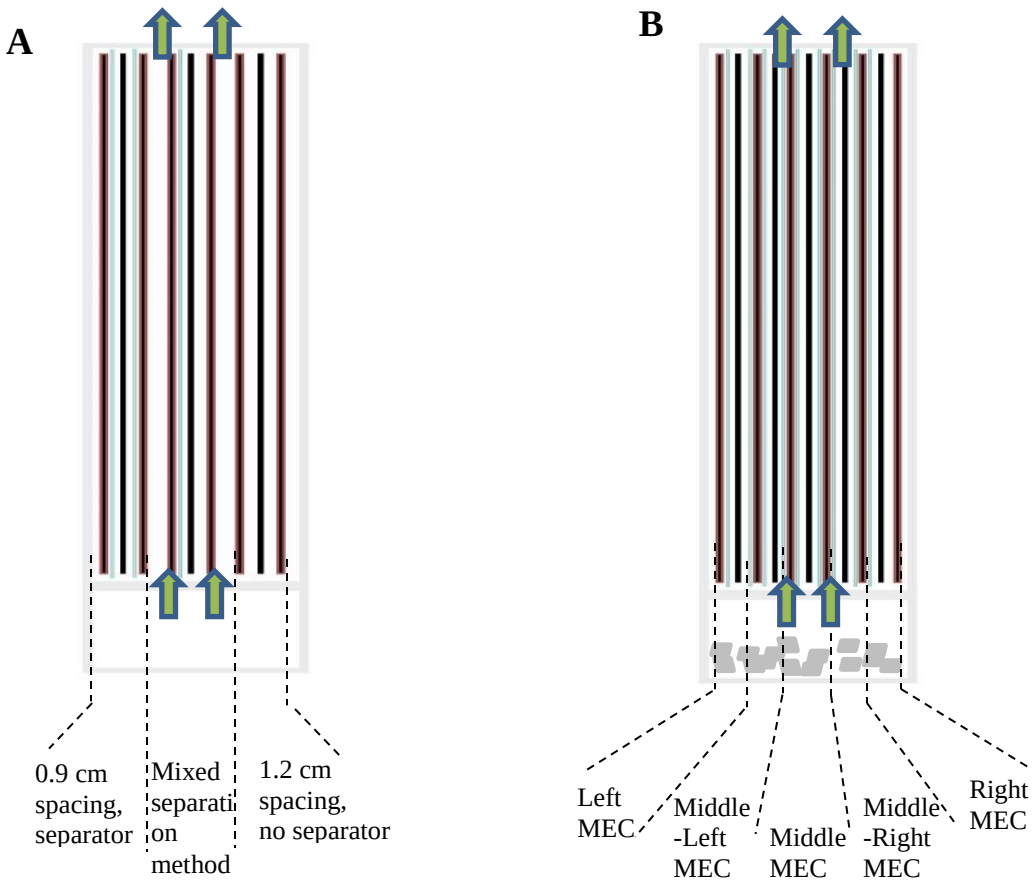

Figure 3.2: Diagram of reactor electrode configurations with recirculation inlets and outlets - green arrows; anode set - red; cathode – black; separator – blue (A) 3C (B) 5C with fermentative beads in bottom – gray

3.2.6 Performance Calculations

Current density was calculated by dividing the current measured between each cathode and the power supply by its surface area (563 cm^2 or 0.0563 m^2). Surface area to volume ratios were calculated by dividing the projected surface area of the cathode in a given configuration by the working volume of the reactor (10 L or 0.01 m^3). The cathodic H_2 recovery and the energy yield relative to the electrical input were calculated as described previously (Logan et al., 2008). A gas temperature of 23°C (300K) was used, as gas volumes were measured at room

temperature. The higher heat of combustion, 285.83 kJ/mol-H_2, was used for the energy yield calculation.

3.3 RESULTS AND DISCUSSION

3.3.1 Impact of Wiring Choice on Current Output

During startup of the reactor, the cathode and anode frames were initially connected to stainless steel and titanium wires, respectively (Fig. 3.3). These wires extended outside of the reactor body, where they were connected to the power supply using copper stranded wire. Stainless steel and titanium were used, in order to match the composition of the electrode frames, and because stainless steel is a suitable cathode material and titanium is well known to resist oxidative corrosion at the anode (Logan, 2010; Su et al., 2016). However, the wires, which were on the order of ten centimeters long, were causing a large voltage drop, since they were transmitting all of the current that was collected at the large-surface-area cathode or anode set. For a 30 A/m^2 current density that is collected through a wire on each electrode, the high resistivity of stainless steel (6.9×10^{-7} Ω m) and titanium (4.20×10^{-7} Ω m) cause a voltage drop of around 0.3 V and 0.2 V, respectively (Helmenstine and Ph.D., n.d.). It is best to keep input voltages low for economic reasons, and this is a very significant voltage loss, considering that input voltages are typically in the range of 0.7 – 1 V (Kadier et al., 2016).

Options to resolve this ‘traffic jam’ in the electrical current included increasing the number or thickness of wires that connect to each frame or changing the material of the wire.

Since copper has about 30 times the conductivity of titanium and stainless steel, the wires were replaced with stranded copper wires (Helmenstine and Ph.D., n.d.). This change enabled current to increase to a much higher level (Fig. 3.3), with 5.5 A of total current being equivalent to an average cathodic current density of 32 A/m^2. However, these stranded wires were found to become brittle and fragile after a period of operation of about 45 days, and they were replaced with 18 gauge solid-core copper wire. The electrical performance of these solid-core copper wires was indistinguishable from the stranded copper wires, and they did not appear to deteriorate mechanically over the course of about 35 days.

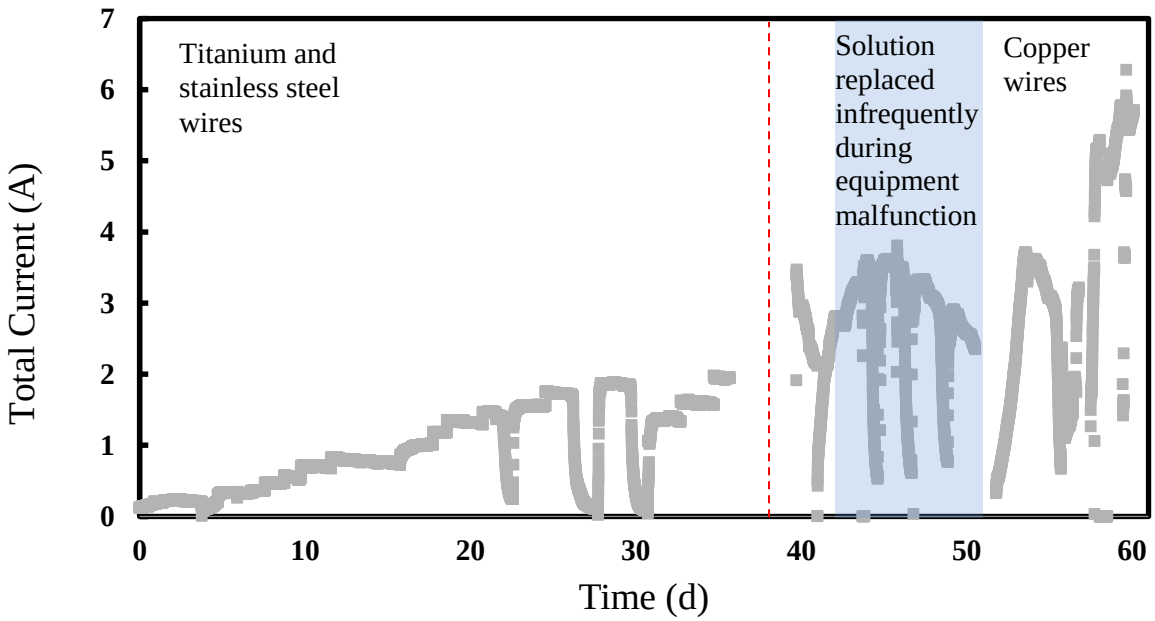

Figure 3.3: Startup of MEC reactor (3C configuration) showing change of electrode wiring – red dashed line, from titanium and stainless steel to stranded copper

3.3.2 Influence of Cloth Separator and Electrode Spacing

The 3C reactor was set up so that the two MECs on the sides would be as similar to each other as possible, except for the way that the anode and cathode were separated (Fig. 3.2A). The current density of MECs with fewer separators was consistently higher than the current density of MECs with separators on more sides of the cathode (Fig. 3.4). However, this observed difference could be due to at least two possible reasons, which have opposite implications for the advantage of one method over the other. The first possible reason is that the wide spacings and lack of cloth barrier encouraged more fluid flow and mixing which, along with the lack of separator itself, improved chemical transfer between the electrodes. The second possibility is that the anodes and cathodes that do not have separators between them had some electrical contact between them. Electrical contact, such as through direct contact of the two electrodes with each other, causes a portion of the current to not produce H_2 gas. The portion of the current caused by an electrical current would pass from the cathode to the anode as electrons, rather than from the anode to the cathode as H^+ ions. It is not possible from this study to definitively state that wider electrode spacing and lack of cloth separator increased H_2-producing current by about 30%, but the clear trend and reasonable values of current density make this likely.

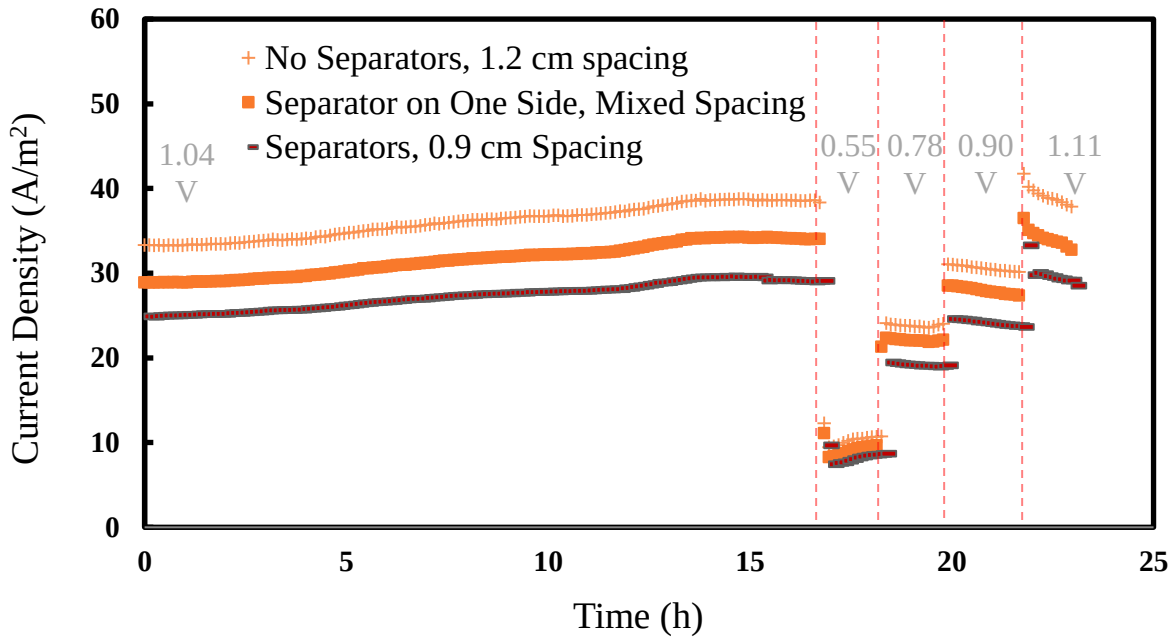

Figure 3.4: Reactor operated in 3C configuration at a range of input voltages
Substrate - Acetate (50 mM) ; HRT - 24 h ; Buffer – Phosphate Solution (100 mM)

3.3.3 Effect of MEC Location in Reactor

Multi-electrode reactors are anticipated to be required for MEC scale-up, so it is useful to research the ways that MECs within a single reactor affect the performance of each other (Rader and Logan, 2010). An additional consideration for scale-up is whether a particular reactor design enables MECs in all locations of the reactor to perform well. In our study, the multi-electrode interaction and the effect of location within the reactor vary based on hydraulic retention time (HRT) (Fig. 3.5). With a 12 h HRT the middle three MECs performed nearly equivalently, in terms of current density, whereas with a 24 h HRT the current densities of each of these three MECs were more distinct from each other. In contrast, the side MECs, ‘Left’ and ‘Right’, remained low and high, respectively, during both HRTs.

A 12 h HRT provided sufficient substrate for the MECs to perform at a maximum current density for the given input voltage, since decreasing the retention time to 6 h did not further improve performance (data not shown). However, when an HRT of 24 h was used the performance of each individual MEC was lower (Fig. 3.5). This implies that substrate availability was limiting performance when the HRT was 24 h, but not when it was 12 h. When there was sufficient substrate the middle three MECs performed equivalently well, showing very similar current densities, whereas when it was limiting they performed more differently from each other and at a lower level. This may be due to competition for substrate, where one MEC performing at a higher rate is lowering the substrate concentration in the area, causing MECs in the vicinity to perform at a lower rate. So, recirculating the liquid at about 0.6 L/L-reactor/h at two locations per three MECs was found to equalize access to substrate, at least for higher loading rates.

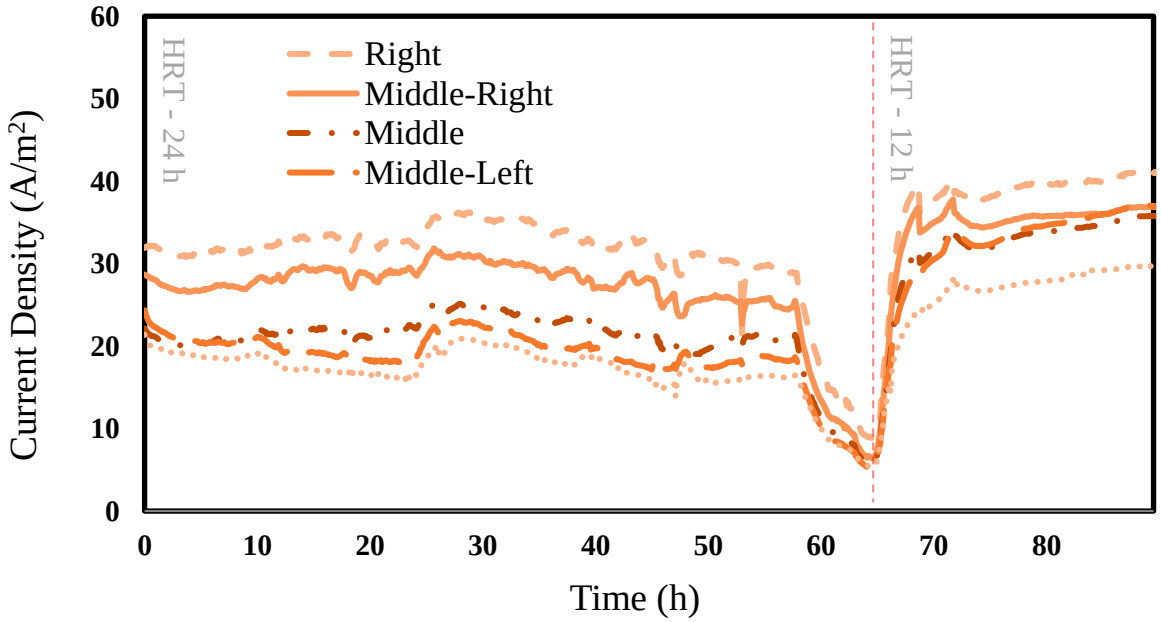

Figure 3.5: Reactor operated in 5C configuration at 24 h retention time and 12 h retention time Substrate - Acetate (50 mM) & Glucose (2 g/l) ; Buffer – Bicarbonate Solution (100 mM); Input Voltage: 1.0 V

The Right MEC had a consistently higher current density than the other MECs, which was likely explained by the way that its anode sets were separated from its cathode. The Right MEC was the only MEC in the 5C configuration that lacked separator cloth and had a wider spacing between the anode sets and the cathode. This means that conclusions about MEC interaction and effect of location were not drawn from the performance of the Right MEC, but it was included for the sake of completeness. The left MEC, on the other hand, was designed to be the same as the three middle MECs, except for its proximity to the wall of the reactor. Since it consistently displayed a lower current density than the three middle MECs, there is some evidence that for this reactor design, the MECs located next to the walls experienced a decrease in performance of about 20%. It is hypothesized that this is due to negative effects that the wall has on fluid motion and therefore mixing.

3.3.4 H_2-Production Performance

The 3C configuration produced 3.85 L/L/d for a period of about 1 day (22 h) while operating with acetate as substrate and with a 24 h retention time. This corresponded with to a cathodic H_2 recovery of about 0.67. Assuming that all acetate was consumed this makes a H_2 yield of about 3.1 mol-H_2/mol-acetate, compared to the ideal value of 4 mol-H_2/mol-acetate. The yield of energy contained within in H_2 fuel relative to the amount of input electricity was 0.94. The 5C configuration had a H_2-production rate of 5.92 L/L/d over a period of 18 h, with a retention time of 12 h. The substrates used for this test were acetate (50 mM) and glucose (2 g/L), and the H_2 produced by the MECs was potentially supplemented by H_2 from the fermentation of glucose by the immobilized bacterial beads. Considering the total amount of H_2

produced and the amount of electrical current through the system, the cathodic H_2 recovery for this test was about 0.56. The yield of energy relative to the electrical input was 0.82. In other studies homoacetogenesis was found to strongly lower H_2-production through H_2-consumption (Xafenias and Mapelli, 2014). For both of these two tests $CHCl_3$ (0.02% volume/volume) was added to the solution to control homoacetogenesis.

3.3.5 Effect of Scale-Up on Current Density

For the same tests that were analyzed for H_2-production, the current density (by cathode surface area, averaged between the multiple MECs) was 30.8 A/m^2 (3C configuration; input voltage 1.06 V; acetate concentration 50 mM; HRT 24 h; phosphate buffer concentration 100 mM) and 34.4 A/m^2 (5C configuration; input voltage 1.0 V; acetate concentration 50 mM; glucose concentration: 2 g/L; HRT 12 h; bicarbonate buffer concentration 150 mM). The current density achieved with the 3C configuration was compared to the current density of predicted from an internal resistance analysis of small-scale MECs (volume 0.15 L; cathode surface area 15 cm^2). The predicted current density was based on the surface area of the carbon cloth electrodes, the buffer concentration of the solution, the input voltage, and a qualitative assessment of the level of solution mixing between the electrodes. The ‘high’ and ‘low’ mixing condition are estimates of the maximum and minimum easily-achievable mixing condition for this parallel-electrode design. The high mixing condition was created by operating the small-scale MECs on a shake plate that is oscillating at 90 rpm and with a diameter of revolution of 10 mm. The low mixing condition was created by operating the MECs in a stationary (non-shaking) mode, where there was no large cause for fluid motion within the MECs. The predicted current

density for the 3C configuration in both of these two mixing conditions is plotted alongside the observed current density of each cathode during 85 minutes of testing at four applied voltages (Fig. 3.6). Nearly all of the current density values fall within the range of predicted values between the two mixing conditions. The fluid motion within the larger MEC reactor was likely greater than that of the stationary (non-mixing) small-scale MECs, but less than the shaking MECs. Dividing the recirculation rate (100 mL/min or 1.7×10^{-7} m^3/s) by the cross-sectional area (0.0084 m^2) reveals that the average upward flow speed was about 0.0002 m/s or 0.2 mm/s. A flow of this speed is barely noticeable to the naked eye, as opposed to the obvious fluid motion within the shaking small-scale MECs. However, in the larger MEC reactor, fluid shear and mixing caused by the rising of gas bubbles may have been more significant than the fluid motion caused by recirculation. The shear rate due to recirculation, estimated by dividing upward flow speed by half of the gap between the electrodes, was about 0.04 s^{-1}, whereas shear rates in bubble column reactors were found to be much larger in general (0.2 – 1000 s^{-1}) (Chisti and Moo-Young, 1989). The spread of the current density values within the mixing condition 'window' provides further evidence that the MECs without separator cloth and with wider spacing had improved fluid flow and chemical transport, compared to the MECs separated with the cloth. Current density as a metric of performance is comparable between the mid-size reactor and a small-scale reactor.

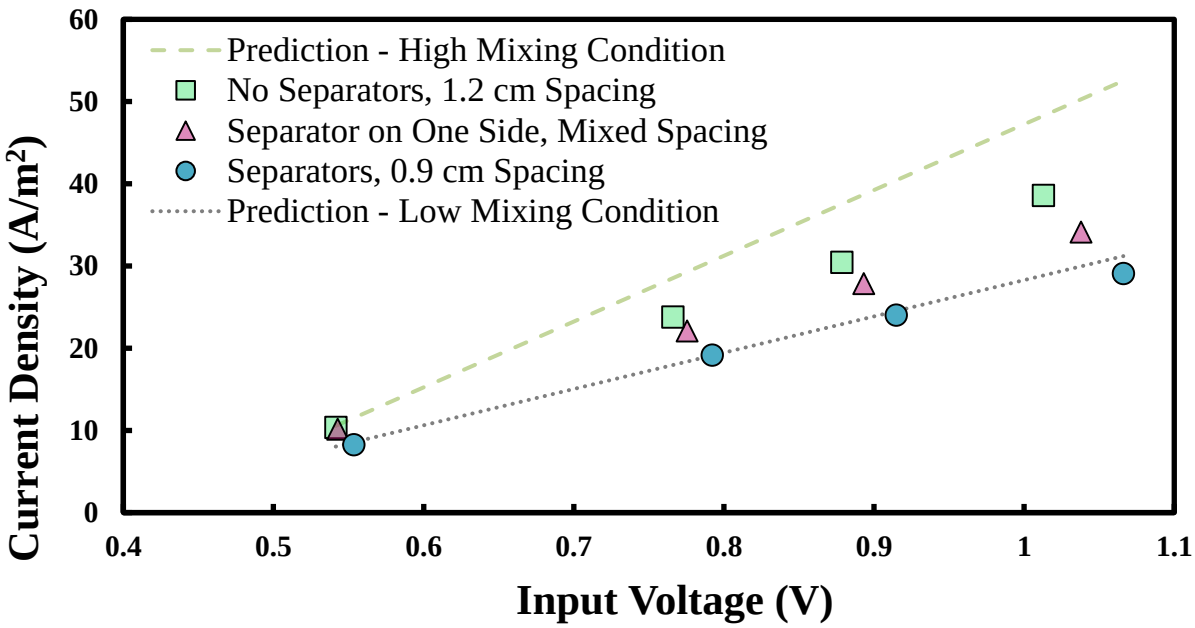

Fig. 3.6: Current density predicted based on the MEC design, for high and low mixing condition, compared to the measured values for the 3C configuration; Substrate - Acetate (50 mM) ; HRT - 24 h ; Buffer – Phosphate Solution (100 mM)

3.4 IMPLICATIONS

The MEC reactor in our study was designed to be scalable and high performance. With these goals in mind, the single-chamber and membrane-less reactor had the following features:

- 10 L reactor with high current density and H_2-production rates
- Electrical performance scaled directly from small (0.15 L) MECs
- Competitive surface area to volume ratio
- High height to width of the MEC to encourage fluid mixing
- Sheet metal electrode frames to provide distributed electrical connection
- Solid-core insulated copper wires to collect electrode current effectively

By extending the width of the rectangular cross-section, more MECs can be added in, to be able to treat a larger waste stream. With a greater number of MECs in a single reactor, a smaller percentage of them will be located at the sides (two MECs, no matter the reactor width). For this reason, the lower performance of the side MECs will not be a big issue for scale-up with this design. If, for future reactors, it can be guaranteed that the anodes will not touch the cathodes, then it is recommended to keep them spaced from each other by about one centimeter, without the use of separator cloth. The separator cloth, and the smaller electrode spacing that it enabled, was found to likely decrease performance due to diminished fluid mixing.

A surface area to volume ratio of about 28 m^2/m^3 was achieved with the 5C configuration, and a ratio more than an estimated 50% higher than this value may not be feasible with our reactor design. However, adding two cathodes (5C configuration compared to 3C configuration) did not noticeably decrease the current density, indicating that there is no significant tradeoff when increasing MEC density within the reactor. Further support for the benefit of increasing the number of MECs in this reactor is that the hydrogen production rate increased about 54% (from 3.8 to 5.9 L/L-reactor/d) with a 67% increase in surface area to volume ratio (from 17 to about 28 m^2/m^3), although the operating conditions are not identical (3C configuration: substrate – 50 mM acetate, HRT – 24 h ; 5C configuration: substrate – 50 mM acetate and 2g/L glucose, HRT – 12 h). As long as the design presented here continues to compare favorably with other MEC reactors of similar size, research will focus on decreasing the cost of the most expensive components and testing various waste streams with pilot-scale reactors. The carbon cloth in the electrodes may be able to be replaced with cheaper materials, such as carbon felt. Similarly, future study will test whether plastic frames with titanium and stainless steel foil glued to the surface can replace the sheet metal electrode frames.

3.5 REFERENCES

Bond, D.R., Lovley, D.R., 2003. Electricity Production by Geobacter sulfurreducens Attached to Electrodes. Appl. Environ. Microbiol. 69, 1548–1555. https://doi.org/10.1128/AEM.69.3.1548-1555.2003

Cheng, S., Logan, B.E., 2007. Sustainable and efficient biohydrogen production via electrohydrogenesis. Proc. Natl. Acad. Sci. 104, 18871–18873. https://doi.org/10.1073/pnas.0706379104

Chisti, Y., Moo-Young, M., 1989. On the calculation of shear rate and apparent viscosity in airlift and bubble column bioreactors. Biotechnol. Bioeng. 34, 1391–1392. https://doi.org/10.1002/bit.260341107

Cotterill S. E., Dolfing J., Jones C., Curtis T. P., Heidrich E. S., 2017. Low Temperature Domestic Wastewater Treatment in a Microbial Electrolysis Cell with 1 m2 Anodes: Towards System Scale-Up. Fuel Cells 17, 584–592. https://doi.org/10.1002/fuce.201700034

Cusick, R.D., Bryan, B., Parker, D.S., Merrill, M.D., Mehanna, M., Kiely, P.D., Liu, G., Logan, B.E., 2011. Performance of a pilot-scale continuous flow microbial electrolysis cell fed winery wastewater. Appl. Microbiol. Biotechnol. 89, 2053–2063. https://doi.org/10.1007/s00253-011-3130-9

Escapa, A., Mateos, R., Martínez, E.J., Blanes, J., 2016. Microbial electrolysis cells: An emerging technology for wastewater treatment and energy recovery. From laboratory to pilot plant and beyond. Renew. Sustain. Energy Rev. 55, 942–956. https://doi.org/10.1016/j.rser.2015.11.029

Gil-Carrera, L., Escapa, A., Mehta, P., Santoyo, G., Guiot, S.R., Morán, A., Tartakovsky, B., 2013. Microbial electrolysis cell scale-up for combined wastewater treatment and hydrogen production. Bioresour. Technol. 130, 584–591. https://doi.org/10.1016/j.biortech.2012.12.062

Guo, K., Prévoteau, A., Rabaey, K., 2017. A novel tubular microbial electrolysis cell for high rate hydrogen production. J. Power Sources 356, 484–490. https://doi.org/10.1016/j.jpowsour.2017.03.029

Hawkes, F.R., Hussy, I., Kyazze, G., Dinsdale, R., Hawkes, D.L., 2007. Continuous dark fermentative hydrogen production by mesophilic microflora: Principles and progress. Int. J. Hydrog. Energy 32, 172–184. https://doi.org/10.1016/j.ijhydene.2006.08.014

Helmenstine, A.M., Ph.D., n.d. Know the Electrical Conductivity and Resistivity of Common Materials [WWW Document]. ThoughtCo. URL https://www.thoughtco.com/table-of-electrical-resistivity-conductivity-608499 (accessed 5.23.18).

Hou, Y., Zhang, R., Luo, H., Liu, G., Kim, Y., Yu, S., Zeng, J., 2015. Microbial electrolysis cell with spiral wound electrode for wastewater treatment and methane production. Process Biochem. 50, 1103–1109. https://doi.org/10.1016/j.procbio.2015.04.001

Kadier, A., Kalil, M.S., Abdeshahian, P., Chandrasekhar, K., Mohamed, A., Azman, N.F., Logroño, W., Simayi, Y., Hamid, A.A., 2016. Recent advances and emerging challenges in microbial electrolysis cells (MECs) for microbial production of hydrogen and value-added chemicals. Renew. Sustain. Energy Rev. 61, 501–525. https://doi.org/10.1016/j.rser.2016.04.017

Liu, H., Logan, B.E., 2004. Electricity Generation Using an Air-Cathode Single Chamber Microbial Fuel Cell in the Presence and Absence of a Proton Exchange Membrane. Environ. Sci. Technol. 38, 4040–4046. https://doi.org/10.1021/es0499344

Logan, B.E., 2010. Scaling up microbial fuel cells and other bioelectrochemical systems. Appl. Microbiol. Biotechnol. 85, 1665–1671. https://doi.org/10.1007/s00253-009-2378-9

Logan, B.E., Call, D., Cheng, S., Hamelers, H.V.M., Sleutels, T.H.J.A., Jeremiasse, A.W., Rozendal, R.A., 2008. Microbial Electrolysis Cells for High Yield Hydrogen Gas Production from Organic Matter. Environ. Sci. Technol. 42, 8630–8640. https://doi.org/10.1021/es801553z

Lu, L., Xing, D., Liu, B., Ren, N., 2012. Enhanced hydrogen production from waste activated sludge by cascade utilization of organic matter in microbial electrolysis cells. Water Res. 46, 1015–1026. https://doi.org/10.1016/j.watres.2011.11.073

Rader, G.K., Logan, B.E., 2010. Multi-electrode continuous flow microbial electrolysis cell for biogas production from acetate. Int. J. Hydrog. Energy 35, 8848–8854. https://doi.org/10.1016/j.ijhydene.2010.06.033

Ramachandran, R., Menon, R.K., 1998. An overview of industrial uses of hydrogen. Int. J. Hydrog. Energy 23, 593–598. https://doi.org/10.1016/S0360-3199(97)00112-2

Su, M., Wei, L., Qiu, Z., Wang, G., Shen, J., 2016. Hydrogen production in single chamber microbial electrolysis cells with stainless steel fiber felt cathodes. J. Power Sources 301, 29–34. https://doi.org/10.1016/j.jpowsour.2015.09.108

Wu, S.-Y., Lin, C.-N., Chang, J.-S., Lee, K.-S., Lin, P.-J., 2002. Microbial Hydrogen Production with Immobilized Sewage Sludge. Biotechnol. Prog. 18, 921–926. https://doi.org/10.1021/bp0200548

Xafenias, N., Mapelli, V., 2014. Performance and bacterial enrichment of bioelectrochemical systems during methane and acetate production. Int. J. Hydrog. Energy 39, 21864–21875. https://doi.org/10.1016/j.ijhydene.2014.05.038

Chapter 4: Conclusions

This work serves as a focused investigation of the way that the physical setup of a single-chamber MEC affects its performance. Since MECs are low-voltage (~1 volt), high-current (multiple amps at 10 L –scale) devices, it is crucial to keep all resistances within the system as low as possible. A resistance associated with a component or a process that is much larger than the other resistances will govern the overall performance, so this 'limiting-factor' must be remedied before the effect of any other design change can be assessed well. The design and operation factors that most limited performance were found to be:

1) Anode surface area
2) Fluid mixing condition (comparable)
3) Solution buffer concentration (comparable)

Surprisingly, electrode spacing was not found to have a large impact on performance (phosphate buffer concentration: 30 – 200 mM), contrary to what has been found by other studies and what is the general thought in the field. The most likely reason for this difference in results was the range of electrode distances tested (4 – 9 mm), since other studies tested electrode spacing distances of multiple centimeters. This suggests either that the resistance associated with small electrode distances (< 1 cm) were small enough that further decrease did not have a large overall effect, or that decreasing this resistance has a tradeoff with another resistance (eg. worsening the mixing condition).

The results of the limiting-factor analysis was used to inform the design of a 10 L reactor. Achieving a sufficient mixing condition within the reactor was prioritized over keeping electrode spacing distances low, so distances of 0.9 cm and 1.2 cm were used. For mixing purposes, the solution was recirculated at a rate of 0.6 L/L-reactor/h through the electrodes with two inlets and outlets. Increasing the recirculation rate to 1 L/L-reactor/h did not appear to improve performance. A successful large reactor must also be designed for the current to be collected from the anode and distributed to the cathode with little voltage loss. This is different from small-scale reactors, which have low current and therefore lower voltage drop in the wires that connect to the electrodes. This was achieved in two ways, by clamping the carbon cloth electrodes in sheet metal frames and connecting those frames with wiring outside of the reactor using solid-core copper wires. Stainless steel and titanium wires, as well as stranded copper wires were all tested, but were found to be inadequate, unlike the insulated 18 gauge solid copper wires. The reactor achieved a current density (970 A/m^3) higher than all values found for reactors larger than 1 L, to the best of our knowledge. The H_2-production rate at the same condition was high, at 5.9 L/L/d (5C configuration; input voltage 1.0 V; acetate concentration 50 mM; glucose concentration: 2 g/L; HRT 12 h; bicarbonate buffer concentration 150 mM). This was due mostly to high performance based on electrode surface area, rather than on a higher density of electrode surface area within the reactor, since the surface area to volume ratio (30 m^2-cathode/m^3-reactor) was similar to published designs. The MEC reactor design is scalable by extending the width of the reactor to add in more electrode pairs.

The input voltage was found to scale linearly with the MEC current, allowing a single internal resistance value to be determined for each MEC design. Additionally, the internal resistance was successfully split into three parts based on four design settings: anode surface

area; cathode surface area; solution buffer concentration; and mixing condition (high/low). This gives researchers a tool to get a sense of whether an electrode surface area or the buffer concentration is limiting performance, and if there is likely room to improve their fluid mixing condition. The model is for single-chamber MECs with carbon cloth cathodes containing high-performance catalyst, and with carbon-based anodes. The design decision internal resistance results were useful for picking an appropriate ratio of anode surface area to cathode surface area for the 10 L MEC reactor (5C configuration - 3.6:1) based on the finding that a ratio of 3-3.5 : 1 balanced the anode and cathode resistances. Additionally, the internal resistance model was used to confirm that the electrical performance of the 10 L scaled directly from the small-scale (0.15 L) reactors. Lastly, the internal resistance model suggested that improved mixing condition was the reason for higher current densities achieved by electrode pairs separated without a cloth separator.

The reactor designed and tested in this work did not use precious metals, which is an important step toward lowering the capital cost of MECs. However, further testing of cheaper materials to determine their suitability for use in MEC reactors will continue to increase their practicality. Secondly, ongoing research on methods to control H_2-consumption, such as the chemical method used in this study, will complement all other MEC research and make it so that simple, single-chamber designs can be high performing. Finally, operation of MEC reactors with many different waste streams will clarify the role in which this technology fits best.

Bibliography

Ajayi, F.F., Kim, K.-Y., Chae, K.-J., Choi, M.-J., Kim, I.S., 2010. Effect of hydrodymamic force and prolonged oxygen exposure on the performance of anodic biofilm in microbial electrolysis cells. Int. J. Hydrog. Energy 35, 3206–3213. https://doi.org/10.1016/j.ijhydene.2010.01.057

Barbosa, S.G., Peixoto, L., Soares, O.S.G.P., Pereira, M.F.R., Heijne, A.T., Kuntke, P., Alves, M.M., Pereira, M.A., 2018. Influence of carbon anode properties on performance and microbiome of Microbial Electrolysis Cells operated on urine. Electrochimica Acta 267, 122–132. https://doi.org/10.1016/j.electacta.2018.02.083

Bond, D.R., Lovley, D.R., 2003. Electricity Production by Geobacter sulfurreducens Attached to Electrodes. Appl. Environ. Microbiol. 69, 1548–1555. https://doi.org/10.1128/AEM.69.3.1548-1555.2003

Brown, R.K., Harnisch, F., Dockhorn, T., Schröder, U., 2015. Examining sludge production in bioelectrochemical systems treating domestic wastewater. Bioresour. Technol. 198, 913–917. https://doi.org/10.1016/j.biortech.2015.09.081

Brown, R.K., Harnisch, F., Wirth, S., Wahlandt, H., Dockhorn, T., Dichtl, N., Schröder, U., 2014. Evaluating the effects of scaling up on the performance of bioelectrochemical systems using a technical scale microbial electrolysis cell. Bioresour. Technol. 163, 206–213. https://doi.org/10.1016/j.biortech.2014.04.044

Büchs, J., Maier, U., Milbradt, C., Zoels, B., 2000. Power consumption in shaking flasks on rotary shaking machines: I. Power consumption measurement in unbaffled flasks at low liquid viscosity. Biotechnol. Bioeng. 68, 589–593. https://doi.org/10.1002/(SICI)1097-0290(20000620)68:6<589::AID-BIT1>3.0.CO;2-J

Call, D., Logan, B.E., 2008. Hydrogen Production in a Single Chamber Microbial Electrolysis Cell Lacking a Membrane. Environ. Sci. Technol. 42, 3401–3406. https://doi.org/10.1021/es8001822

Cheng, S., Logan, B.E., 2011. High hydrogen production rate of microbial electrolysis cell (MEC) with reduced electrode spacing. Bioresour. Technol. 102, 3571–3574. https://doi.org/10.1016/j.biortech.2010.10.025

Cheng, S., Logan, B.E., 2007. Sustainable and efficient biohydrogen production via electrohydrogenesis. Proc. Natl. Acad. Sci. 104, 18871–18873. https://doi.org/10.1073/pnas.0706379104

Chisti, Y., Moo-Young, M., 1989. On the calculation of shear rate and apparent viscosity in airlift and bubble column bioreactors. Biotechnol. Bioeng. 34, 1391–1392. https://doi.org/10.1002/bit.260341107

Cotterill S. E., Dolfing J., Jones C., Curtis T. P., Heidrich E. S., 2017. Low Temperature Domestic Wastewater Treatment in a Microbial Electrolysis Cell with 1 m2 Anodes:

Towards System Scale-Up. Fuel Cells 17, 584–592. https://doi.org/10.1002/fuce.201700034

Cusick, R.D., Bryan, B., Parker, D.S., Merrill, M.D., Mehanna, M., Kiely, P.D., Liu, G., Logan, B.E., 2011. Performance of a pilot-scale continuous flow microbial electrolysis cell fed winery wastewater. Appl. Microbiol. Biotechnol. 89, 2053–2063. https://doi.org/10.1007/s00253-011-3130-9

Cusick, R.D., Kiely, P.D., Logan, B.E., 2010. A monetary comparison of energy recovered from microbial fuel cells and microbial electrolysis cells fed winery or domestic wastewaters. Int. J. Hydrog. Energy 35, 8855–8861. https://doi.org/10.1016/j.ijhydene.2010.06.077

Dominguez-Benetton, X., Sevda, S., Vanbroekhoven, K., Pant, D., 2012. The accurate use of impedance analysis for the study of microbial electrochemical systems. Chem. Soc. Rev. 41, 7228–7246. https://doi.org/10.1039/C2CS35026B

Dudley, H.J., Lu, L., Ren, Z.J., Bortz, D.M., 2018. Sensitivity and Bifurcation Analysis of a DAE Model for a Microbial Electrolysis Cell. ArXiv180206326 Math Q-Bio.

Escapa, A., Mateos, R., Martínez, E.J., Blanes, J., 2016. Microbial electrolysis cells: An emerging technology for wastewater treatment and energy recovery. From laboratory to pilot plant and beyond. Renew. Sustain. Energy Rev. 55, 942–956. https://doi.org/10.1016/j.rser.2015.11.029

Escapa, A., San-Martín, M.I., Mateos, R., Morán, A., 2015. Scaling-up of membraneless microbial electrolysis cells (MECs) for domestic wastewater treatment: Bottlenecks and limitations. Bioresour. Technol. 180, 72–78. https://doi.org/10.1016/j.biortech.2014.12.096

Fan, Y., Hu, H., Liu, H., 2007. Sustainable Power Generation in Microbial Fuel Cells Using Bicarbonate Buffer and Proton Transfer Mechanisms. Environ. Sci. Technol. 41, 8154–8158. https://doi.org/10.1021/es071739c

Fan, Y., Sharbrough, E., Liu, H., 2008. Quantification of the Internal Resistance Distribution of Microbial Fuel Cells. Environ. Sci. Technol. 42, 8101–8107. https://doi.org/10.1021/es801229j

Gadkari, S., Gu, S., Sadhukhan, J., 2018. Towards automated design of bioelectrochemical systems: A comprehensive review of mathematical models. Chem. Eng. J. 343, 303–316. https://doi.org/10.1016/j.cej.2018.03.005

Gil-Carrera, L., Escapa, A., Mehta, P., Santoyo, G., Guiot, S.R., Morán, A., Tartakovsky, B., 2013. Microbial electrolysis cell scale-up for combined wastewater treatment and hydrogen production. Bioresour. Technol. 130, 584–591. https://doi.org/10.1016/j.biortech.2012.12.062

Gil-Carrera, L., Mehta, P., Escapa, A., Morán, A., García, V., Guiot, S.R., Tartakovsky, B., 2011. Optimizing the electrode size and arrangement in a microbial electrolysis cell. Bioresour. Technol. 102, 9593–9598. https://doi.org/10.1016/j.biortech.2011.08.026

Guo, K., Prévoteau, A., Rabaey, K., 2017. A novel tubular microbial electrolysis cell for high rate hydrogen production. J. Power Sources 356, 484–490. https://doi.org/10.1016/j.jpowsour.2017.03.029

Hawkes, F.R., Hussy, I., Kyazze, G., Dinsdale, R., Hawkes, D.L., 2007. Continuous dark fermentative hydrogen production by mesophilic microflora: Principles and progress. Int. J. Hydrog. Energy 32, 172–184. https://doi.org/10.1016/j.ijhydene.2006.08.014

Helmenstine, A.M., Ph.D., n.d. Know the Electrical Conductivity and Resistivity of Common Materials [WWW Document]. ThoughtCo. URL https://www.thoughtco.com/table-of-electrical-resistivity-conductivity-608499 (accessed 5.23.18).

Hou, Y., Zhang, R., Luo, H., Liu, G., Kim, Y., Yu, S., Zeng, J., 2015. Microbial electrolysis cell with spiral wound electrode for wastewater treatment and methane production. Process Biochem. 50, 1103–1109. https://doi.org/10.1016/j.procbio.2015.04.001

Hu, H., Fan, Y., Liu, H., 2008. Hydrogen production using single-chamber membrane-free microbial electrolysis cells. Water Res. 42, 4172–4178. https://doi.org/10.1016/j.watres.2008.06.015

Jorgensen, K., 2008. Technologies for electric, hybrid and hydrogen vehicles: Electricity from renewable energy sources in transport. Util. Policy, Sustainable Energy and Transportation Systems 16, 72–79. https://doi.org/10.1016/j.jup.2007.11.005

Kadier, A., Kalil, M.S., Abdeshahian, P., Chandrasekhar, K., Mohamed, A., Azman, N.F., Logroño, W., Simayi, Y., Hamid, A.A., 2016. Recent advances and emerging challenges in microbial electrolysis cells (MECs) for microbial production of hydrogen and value-added chemicals. Renew. Sustain. Energy Rev. 61, 501–525. https://doi.org/10.1016/j.rser.2016.04.017

Ki, D., Popat, S.C., Torres, C.I., 2016. Reduced overpotentials in microbial electrolysis cells through improved design, operation, and electrochemical characterization. Chem. Eng. J. 287, 181–188. https://doi.org/10.1016/j.cej.2015.11.022

Lee, H.-S., Rittmann, B.E., 2010. Significance of Biological Hydrogen Oxidation in a Continuous Single-Chamber Microbial Electrolysis Cell. Environ. Sci. Technol. 44, 948–954. https://doi.org/10.1021/es9025358

Liang, D.-W., Peng, S.-K., Lu, S.-F., Liu, Y.-Y., Lan, F., Xiang, Y., 2011. Enhancement of hydrogen production in a single chamber microbial electrolysis cell through anode arrangement optimization. Bioresour. Technol. 102, 10881–10885. https://doi.org/10.1016/j.biortech.2011.09.028

Liu, H., Cheng, S., Logan, B.E., 2005. Power Generation in Fed-Batch Microbial Fuel Cells as a Function of Ionic Strength, Temperature, and Reactor Configuration. Environ. Sci. Technol. 39, 5488–5493. https://doi.org/10.1021/es050316c

Liu, H., Logan, B.E., 2004. Electricity Generation Using an Air-Cathode Single Chamber Microbial Fuel Cell in the Presence and Absence of a Proton Exchange Membrane. Environ. Sci. Technol. 38, 4040–4046. https://doi.org/10.1021/es0499344

Liu, J., Zhang, F., He, W., Yang, W., Feng, Y., Logan, B.E., 2014. A microbial fluidized electrode electrolysis cell (MFEEC) for enhanced hydrogen production. J. Power Sources 271, 530–533. https://doi.org/10.1016/j.jpowsour.2014.08.042

Logan, B.E., 2010. Scaling up microbial fuel cells and other bioelectrochemical systems. Appl. Microbiol. Biotechnol. 85, 1665–1671. https://doi.org/10.1007/s00253-009-2378-9

Logan, B.E., Call, D., Cheng, S., Hamelers, H.V.M., Sleutels, T.H.J.A., Jeremiasse, A.W., Rozendal, R.A., 2008. Microbial Electrolysis Cells for High Yield Hydrogen Gas Production from Organic Matter. Environ. Sci. Technol. 42, 8630–8640. https://doi.org/10.1021/es801553z

Lu, L., Ren, Z.J., 2016. Microbial electrolysis cells for waste biorefinery: A state of the art review. Bioresour. Technol., Waste Biorefinery - Advocating Circular Economy 215, 254–264. https://doi.org/10.1016/j.biortech.2016.03.034

Lu, L., Xing, D., Liu, B., Ren, N., 2012. Enhanced hydrogen production from waste activated sludge by cascade utilization of organic matter in microbial electrolysis cells. Water Res. 46, 1015–1026. https://doi.org/10.1016/j.watres.2011.11.073

Michie, I.S., Kim, J.R., Dinsdale, R.M., Guwy, A.J., Premier, G.C., 2014. The influence of anodic helical design on fluid flow and bioelectrochemical performance. Bioresour. Technol., Special Issue: CESE 2013 & Special Issue: ICABB 2013 165, 13–20. https://doi.org/10.1016/j.biortech.2014.03.069

Parameswaran, P., Torres, C.I., Lee, H.-S., Rittmann, B.E., Krajmalnik-Brown, R., 2011. Hydrogen consumption in microbial electrochemical systems (MXCs): The role of homo-acetogenic bacteria. Bioresour. Technol., Special Issue: Biofuels - II: Algal Biofuels and Microbial Fuel Cells 102, 263–271. https://doi.org/10.1016/j.biortech.2010.03.133

P. Borole, A., J. Lewis, A., 2017. Proton transfer in microbial electrolysis cells. Sustain. Energy Fuels 1, 725–736. https://doi.org/10.1039/C7SE00034K

Rader, G.K., Logan, B.E., 2010. Multi-electrode continuous flow microbial electrolysis cell for biogas production from acetate. Int. J. Hydrog. Energy 35, 8848–8854. https://doi.org/10.1016/j.ijhydene.2010.06.033

Ramachandran, R., Menon, R.K., 1998. An overview of industrial uses of hydrogen. Int. J. Hydrog. Energy 23, 593–598. https://doi.org/10.1016/S0360-3199(97)00112-2

Reclari, M., 2013. Hydrodynamics of orbital shaken bioreactors. ÉCOLE POLYTECHNIQUE FÉDÉRALE DE LAUSANNE.

Rozendal, R.A., Hamelers, H.V.M., Rabaey, K., Keller, J., Buisman, C.J.N., 2008. Towards practical implementation of bioelectrochemical wastewater treatment. Trends Biotechnol. 26, 450–459. https://doi.org/10.1016/j.tibtech.2008.04.008

Sedaqatvand, R., Nasr Esfahany, M., Behzad, T., Mohseni, M., Mardanpour, M.M., 2013. Parameter estimation and characterization of a single-chamber microbial fuel cell for dairy wastewater treatment. Bioresour. Technol. 146, 247–253. https://doi.org/10.1016/j.biortech.2013.07.054

Sleutels, T.H.J.A., Hamelers, H.V.M., Rozendal, R.A., Buisman, C.J.N., 2009a. Ion transport resistance in Microbial Electrolysis Cells with anion and cation exchange membranes. Int. J. Hydrog. Energy 34, 3612–3620. https://doi.org/10.1016/j.ijhydene.2009.03.004

Sleutels, T.H.J.A., Heijne, A.T., Buisman, C.J.N., Hamelers, H.V.M., 2013. Steady-state performance and chemical efficiency of Microbial Electrolysis Cells. Int. J. Hydrog. Energy 38, 7201–7208. https://doi.org/10.1016/j.ijhydene.2013.04.067

Sleutels, T.H.J.A., Lodder, R., Hamelers, H.V.M., Buisman, C.J.N., 2009b. Improved performance of porous bio-anodes in microbial electrolysis cells by enhancing mass and charge transport. Int. J. Hydrog. Energy 34, 9655–9661. https://doi.org/10.1016/j.ijhydene.2009.09.089

Su, M., Wei, L., Qiu, Z., Wang, G., Shen, J., 2016. Hydrogen production in single chamber microbial electrolysis cells with stainless steel fiber felt cathodes. J. Power Sources 301, 29–34. https://doi.org/10.1016/j.jpowsour.2015.09.108

Tan, R.-K., Eberhard, W., Büchs, J., 2011. Measurement and characterization of mixing time in shake flasks. Chem. Eng. Sci. 66, 440–447. https://doi.org/10.1016/j.ces.2010.11.001

Tartakovsky, B., Manuel, M.-F., Wang, H., Guiot, S.R., 2009. High rate membrane-less microbial electrolysis cell for continuous hydrogen production. Int. J. Hydrog. Energy 34, 672–677. https://doi.org/10.1016/j.ijhydene.2008.11.003

Tartakovsky, B., Mehta, P., Santoyo, G., Guiot, S.R., 2011. Maximizing hydrogen production in a microbial electrolysis cell by real-time optimization of applied voltage. Int. J. Hydrog. Energy, International Conference on Hydrogen Production (ICH2P)-2010 36, 10557–10564. https://doi.org/10.1016/j.ijhydene.2011.05.162

Ursua, A., Gandia, L.M., Sanchis, P., 2012. Hydrogen Production From Water Electrolysis: Current Status and Future Trends. Proc. IEEE 100, 410–426. https://doi.org/10.1109/JPROC.2011.2156750

Vilà-Rovira, A., Puig, S., Dolors Balaguer, M., Colprim, J., 2015. Anode hydrodynamics in bioelectrochemical systems. RSC Adv. 5, 78994–79000. https://doi.org/10.1039/C5RA11995B

Wilson, E.L., Kim, Y., 2016. The yield and decay coefficients of exoelectrogenic bacteria in bioelectrochemical systems. Water Res. 94, 233–239. https://doi.org/10.1016/j.watres.2016.02.054

Wu, S.-Y., Lin, C.-N., Chang, J.-S., Lee, K.-S., Lin, P.-J., 2002. Microbial Hydrogen Production with Immobilized Sewage Sludge. Biotechnol. Prog. 18, 921–926. https://doi.org/10.1021/bp0200548

Xafenias, N., Mapelli, V., 2014. Performance and bacterial enrichment of bioelectrochemical systems during methane and acetate production. Int. J. Hydrog. Energy 39, 21864–21875. https://doi.org/10.1016/j.ijhydene.2014.05.038

Zhao, L., Li, J., Battaglia, F., He, Z., 2016. Investigation of multiphysics in tubular microbial fuel cells by coupled computational fluid dynamics with multi-order Butler–Volmer reactions. Chem. Eng. J. 296, 377–385. https://doi.org/10.1016/j.cej.2016.03.110

APPENDICES

Appendix A

SMALL-SCALE MEC IMAGES

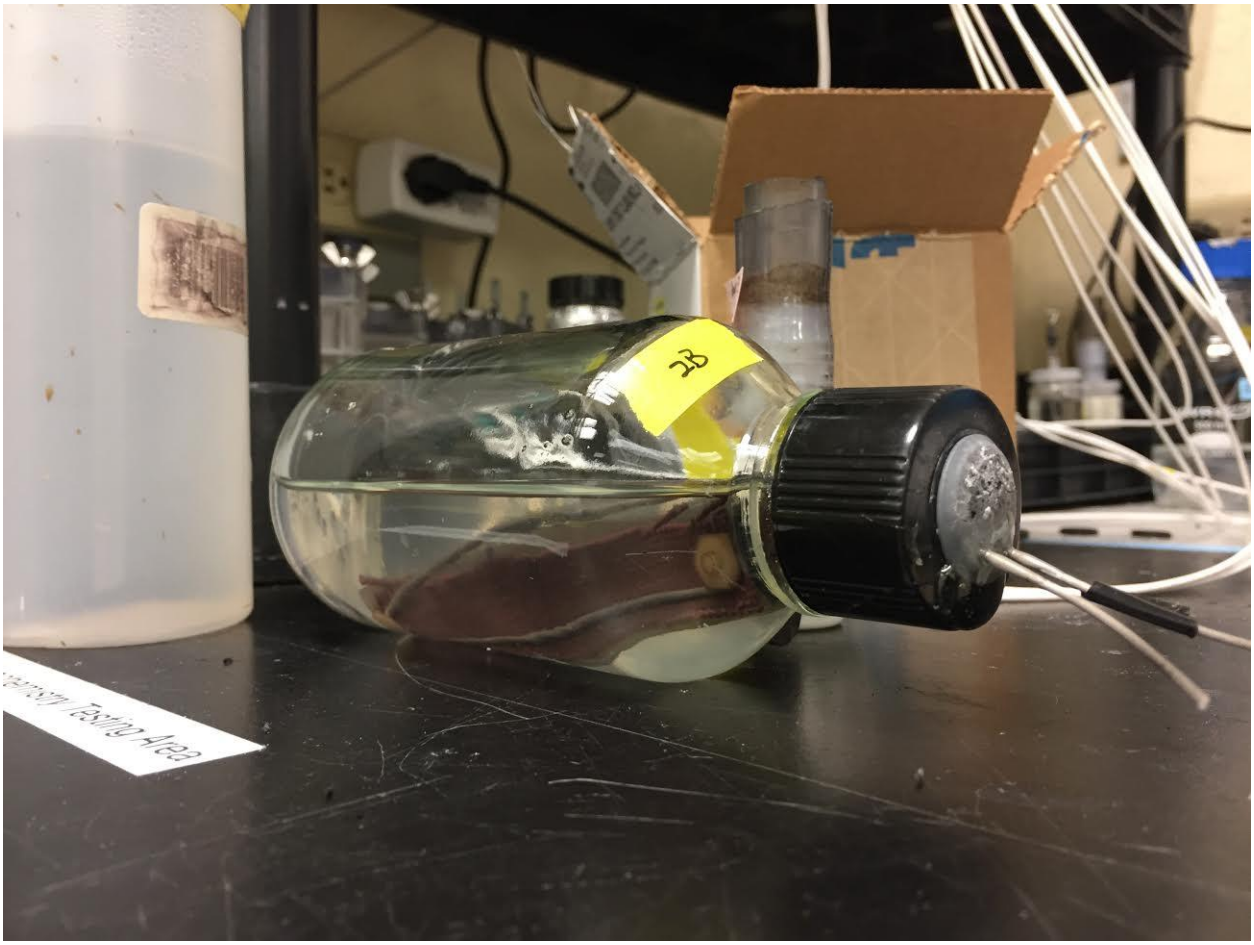

Figure 2.7: Side view of example MEC, showing anode biofilm, titanium wires, and liquid level

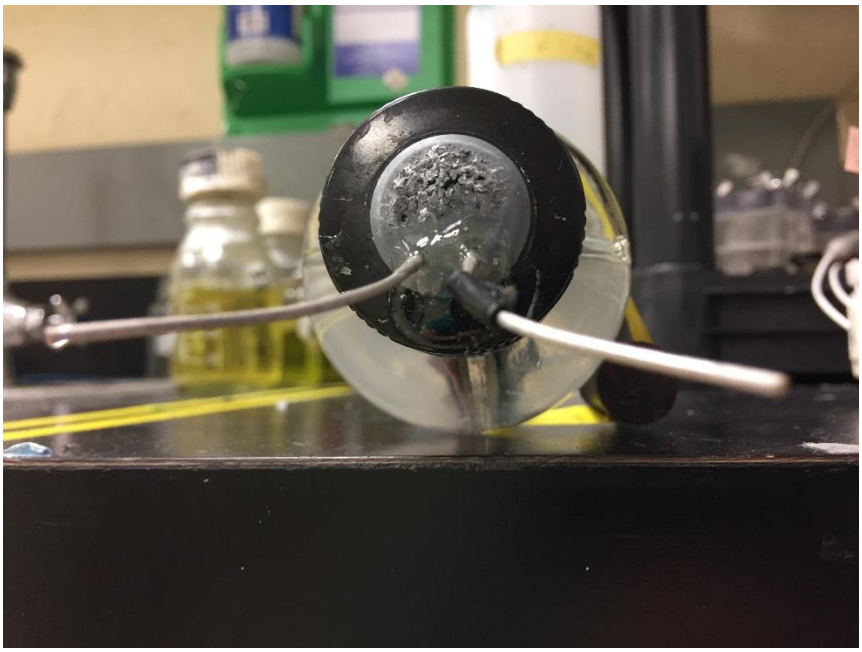

Figure 2.8: Front view of example MEC, showing electrode spacing

CHARACTERIZATION OF FLUID MIXING CONDITION

A study on the influence of mixing using a stir bar on MEC performance has shown that Reynolds number, rather than stirring speed, is the appropriate way to quantify the hydrodynamic flow condition (Ajayi et al., 2010). In that study, as well as in our study, the Reynolds number represents the level of fluid motion that was externally imposed on the fluid within the MEC. In the literature, two separate definitions of Reynolds Numbers were given for bioreactors on shaking orbital plates. The first way that the Reynolds number is defined is shown in Equation 2.8 (Reclari, 2013).

$$Re_1 = \frac{{d_s}^2 * \Omega}{\nu} \tag{2.8}$$

Where d_s is the diameter of the shaking circular trajectory of the shaking plate in [m], Ω is the angular rate of shaking in [rad/s], and ν is the kinematic viscosity of the liquid in [m^2/s]. The second definition was given by Büchs et al. and used by Tan et al. and is shown in Equation 2.9 (Büchs et al., 2000; Tan et al., 2011).

$$Re_2 = \frac{\rho * d^2 * n}{\eta} \tag{2.9}$$

where d is the largest internal diameter of the flask being shaken. Since n (angular shaking rate) is equivalent to Ω in Equation 2.8 and η / ρ (dynamic viscosity of the liquid divided by density of the liquid) is equivalent to ν (kinematic viscosity of the liquid) in Equation 2.8, the two definitions of Reynolds number differ only in their choice of relevant distance value.

For our study the diameter of shaking, d_s , was 1 cm, the angular rate of shaking was 565 rad/s (90 rpm), the largest inner diameter of the MEC, d , was 11.4 cm, and the kinematic viscosity was $8.01*10^{-7}$ m^2/s. Therefore, the Reynolds numbers were 1,200 and 150,000 for Re_1 and Re_2, respectively. The value of Re_2 suggests that the solution within the MEC might have had a mixing time on the order of 7 revolutions, or 5 seconds, although this is not exact, since the MECs were not round shaped and had electrodes which obstructed the flow (Tan et al., 2011). This means that concentration differences between locations in the MEC became approximately homogenized in a matter of seconds, which is much faster than macroscale concentration gradients can form in an MEC. In this way, shaking the MECs likely kept macroscale concentration gradients to negligible levels, which likely improved performance by maintaining

suitable concentrations of substrate or other ions close to all parts of the electrodes (Zhao et al., 2016).

Besides macroscale mixing, shaking also affected the hydrodynamic forces on the electrodes. Profiles of the fluid flow near the electrodes would give an understanding of how much mass transfer is due to fluid motion and how much is due to diffusion. The ratio of the importance of fluid motion and diffusion for a certain species is the Peclet number (Vilà-Rovira et al., 2015). This would also provide information on the shear rate, which was found to affect the level of biofilm formation throughout the depth of the electrode (Michie et al., 2014). However, the flow profiles were not analyzed for this MEC design under shaking or stationary operation.

ELECTROCHEMICAL IMPEDANCE SPECTROSCOPY (EIS) ANALYSIS

The equivalent circuit (Fig. 2.9) contains a resistor, representing ionic/ohmic resistance, in series with two combinations of Constant Phase Elements, resistor and Warburg impedance elements, each combination representing one electrode (P. Borole and J. Lewis, 2017). The resistors within the combinations represent charge transfer resistance, the constant phase elements represent the capacitance of the electrodes, and the Warburg impedance element represents a diffusion layer.

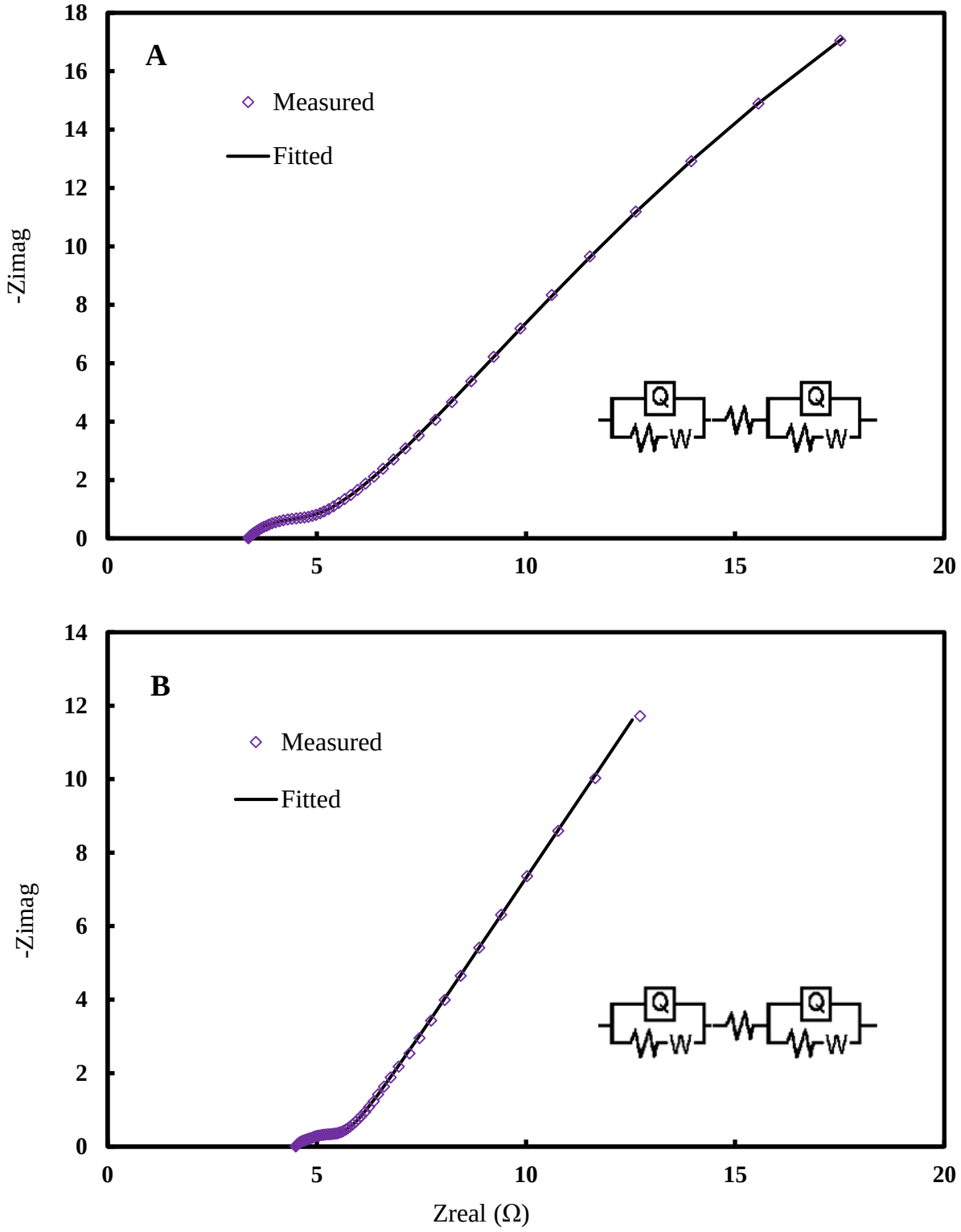

Figure 2.9. Typical EIS Nyquist plot (A) wide-spacing MEC – ohmic resistance 3.7 Ω (B) medium-spacing MEC – ohmic resistance 4.5 Ω

Table 2.2: Ionic/ohmic resistance for small-scale MEC with medium and wide spacing, compared with other studies (PBS = Phosphate Buffer Solution)

	Electrode Spacing or Membrane Type	Substrate	Buffer	Resistance (Ω cm^2)
This Study	0.9 cm	Acetate	75 mM PBS	67
	0.7 cm	Acetate	75 mM PBS	50
Liang et al., 2011	1.5 cm (both anodes on same side)	Acetate	100 mM PBS*	64.0
	1.5 cm (anodes on opposite sides of cathode)	Acetate	100 mM PBS*	42.6
Call and Logan, 2008	~1 – 1.5 cm	Acetate	50 mM PBS	140
	~1 – 1.5 cm	Acetate	200 mM PBS	70
Ki et al., 2016	AEM, Two Chamber (< 0.5 cm) , using Ni cathode	Acetate	Anode chamber: 100 mM PBS ; Cathode Chamber: 100 mM solution of NaCl or NaOH	33
	AEM, Two Chamber (< 0.5 cm) , using SS cathode	Acetate	Anode chamber: 100 mM PBS ; Cathode Chamber: 100 mM solution of NaCl or NaOH	85
P. Borole and J. Lewis, 2017	CEM, Two Chamber	Switchgrass-derived pyrolysis aqueous phase	Anode chamber: 53 mM PBS ; Cathode Chamber: 100 mM PBS	22.3

ASSUMPTIONS ABOUT MECS FOR PERFORMANCE PREDICTION

Table 2.3: Approximation of design of MECs in other studies for use in internal resistance prediction model

	Anode	Approximation of Anode	Cathode	Approximation of Cathode	Buffer	Assumed Mixing Condition
Cheng and Logan 2011	Graphite fiber brushes originally 14 mm in diameter and 25 mm in length, with the edge of the brush anodes were trimmed flat to avoid short circuiting	25 pieces of circular carbon cloth with a diameter of 14 mm – ie. approximating 1 mm of depth as a piece of carbon cloth	Cathodes (7 cm^2) were made of a carbon cloth containing a Pt catalyst (0.5 mg/cm^2)	Carbon cloth (7 cm^2) coated with 2.5 mg/cm^2 MoP	100 mM PBS	Low Mixing Condition (ie. nonshaking)
Liang et al. 2011	Two square pieces of graphite felt (length: 40 mm; width: 35 mm; thickness: 5 mm)	Ten pieces of carbon cloth (40 mm x 35 mm) – ie. approximating 1 mm of depth as a piece of carbon cloth	A square carbon cloth (30 x 22 mm) coated with 0.5 mg/cm^2 platinum	Carbon cloth (30 x 22 mm) coated with 2.5 mg/cm^2 MoP	100 mM PBS*	High Mixing Condition (ie. shaking at 90 rpm)

*Liang et al., 2011 stated that the solution contained 50 mM phosphate buffer, but the recipe listed immediately below was for 100 mM phosphate buffer solution

Appendix B

10 L MEC REACTOR IMAGES

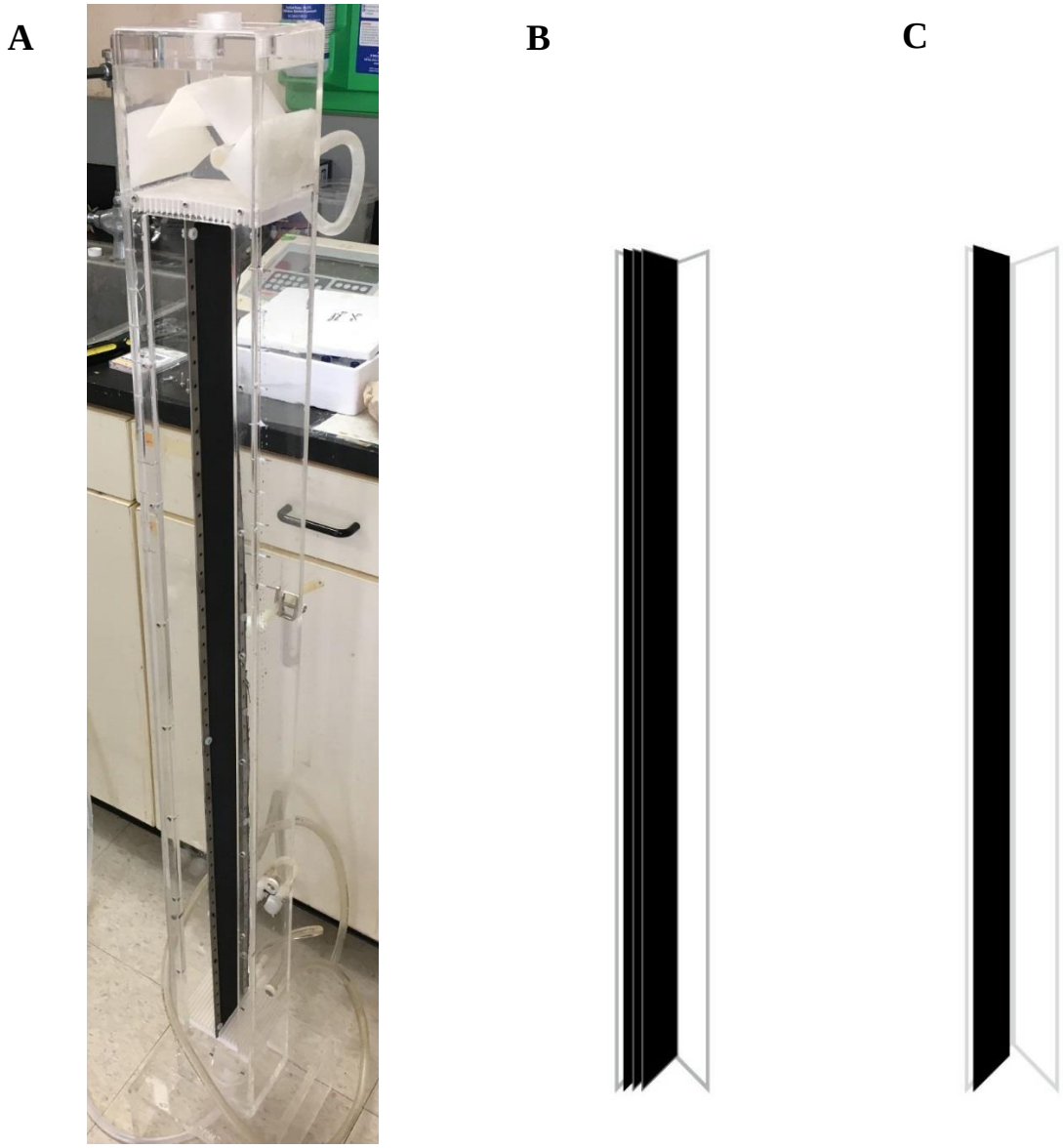

Figure 3.7: (A) 10 L reactor with single electrode to show orientation and diagram of electrodes before clamping (B) anode, showing carbon cloth and titanium frame (C) cathode, showing carbon cloth and stainless steel frame

Figure 3.8: Front view of 5C configuration, showing electrode spacing, separator cloth, fasteners

COMPARISON OF MEC REACTOR PERFORMANCE WITH OTHER STUDIES

Table 3.1: Comparison of 10 L reactor performance with other studies

	Volume [L]	Anode	Cathode	Membrane or Separator	Current Density (Based on Cathode) [A/m^2]	Surface Area to Volume Ratio (Based on Cathode) [m^2/m^3]	Volumetric H_2 Production Rate [L/L-reactor/d]	Volumetric Current Density [A/m^3]	Substrate	Temperature (°C)
Our Study	10	Carbon Cloth	Carbon Cloth	Separator: J-Cloth	31	16.9	3.85	520	Acetate	32
	10	Carbon Cloth	Carbon Cloth	Separator: J-Cloth	34	28.2	5.92	970	Acetate + Glucose	32
(Guo et al., 2017)	1	Pleated Stainless Steel Felt	Platinum-coated Titanium Mesh	Membrane: Anion Exchange	27.8 +/- 0.10	23.6	7.1 +/- 0.01	660	Acetate	35
(Escapa et al., 2015)	6.6	Graphite Felt	Ni-based Gas Diffusion Electrode	Separator: Porous Geotextile	0.3	33.7	~0.01	10	Domestic Waste Water	19.2 +/- 1.1
(Hou et al., 2015)	0.5	Carbon Cloth	Ni Foam	Membrane: Anion Exchange	1.3	60	CH_4: 0.14	78	Acetate + Domestic Waste Water	Room Temperature
(Gil-Carrera et al., 2013)	10	Carbon Felt	Carbon Paper, Ni Gas Diffusion Electrode	Separator: Polyester Cloth	0.616	36.8	0.05	23	Municipal Wastewater	23-25
	0.855	Carbon Felt	Carbon Paper, Ni Gas Diffusion Electrode	Separator: Polyester Cloth	8.14	30.2	2.54 +/- 0.24	246	Simulated High Strength Wastewater	23-25

Table 3.1: Comparison of 10 L reactor performance with other studies (Continued)

	Volume [L]	Anode	Cathode	Membrane or Separator	Current Density (Based on Cathode) [A/m^2]	Surface Area to Volume Ratio (Based on Cathode) [m^2/m^3]	Volumetric H_2 Production Rate [L/L-reactor/d]	Volumetric Current Density [A/m^3]	Substrate	Temperature (°C)
(Rader and Logan, 2010)	2.5	Graphite Fiber Brush	Stainless Steel Mesh	Separator	2.9	24.5	0.53	71	Acetate	30
(Cotteril l S. E. et al., 2017)	175	Graphite Felt	Stainless Steel Wire Wool and Steel Mesh	Membrane: Rhinohide Polyethylene	0.37 +/- 0.23	13	0.003	4.8	Settled Municipal Wastewater	Ambient UK Weather Temperatures
(Brown et al., 2014)	30	Graphite Plates	Stainless Steel Mesh	Membrane: Proton Exchange	0.78 +/- 0.28 Based on Anode	6 Based on Anode	Not Measured	4.7	Acetate	25
	16	Graphite Plates	Stainless Steel Mesh	Membrane: Proton Exchange	1.09 +/- 0.33 Based on Anode	6 Based on Anode	Not Measured	6.5	Acetate + Municipal Wastewater	31 +/- 2
(Cusick et al., 2011)	1000	Graphite Fiber Brushes	Stainless Steel (304) Mesh	Separator: Glass Fiber Matting	1.0	7.2	CH_4: 0.16	7.2	Winery Wastewater	31 +/- 1